respectively). This finding suggested that in HSV-TK expressing cells (HeLa-TK), liposome formulations maintained GCV activity comparable to GCV solution. In HeLa cells, cytotoxicity of GCV-lipo was similar with Empty-lipo. Empty-lipo and PEG-empty-lipo showed some lipid cytotoxicity, and PEG-coating decreased it. HeLa-TK cells seemed to be susceptible to lipid toxicity of Empty-lipo and PEG-empty-lipo than Hela cells. The reason was not clear, but HeLa cells transduced TK might become to be different from those un-treated.

3.5. Pharmacokinetics in normal mice

The pharmacokinetics of PEG-GCV-lipo after intravenous or intraperitoneal injection in ddY mice was examined (Fig. 2). For intravenous or intraperitoneal injection of GCV solution, the disappearance of GCV was so rapid that both injected doses (%) of GCV were very low after 6 h. In contrast, for PEG-GCV-lipo, both injected doses (%) of GCV were about 5% (7.3 and 8.8 μg/ml, respectively) after 12 h. In the absence of PEG-coating, GCV-lipo, 6.2-fold lower levels of GCV than that of PEG-GCV-lipo were found in the blood 3 h after intravenous injection (data not shown). At 3 h post-injection, GCV after intraperitoneal injection was increased to a similar level after intravenous injection, suggesting their rapid dispersion from the peritoneum. For intravenous injection, PEG-GCV-lipo showed about 36-fold higher AUC and lower CL values than GCV solution (Table 3). For intraperitoneal injection, AUC of PEG-GCV-lipo showed about 32-fold higher AUC and lower CL values compared with GCV solution. For intravenous and intraperitoneal injection, terminal half-life ($t_{1/2}$) of PEG-GCV-lipo was 13- and 17-fold higher than GCV solution, respectively. PEG-GCV-lipo showed a long circulation in serum via both injections with prolonged $t_{1/2}$. PEG-GCV-lipo by intravenous injection exhibited 1.2-fold higher AUC value than that by intraperitoneal injection, indicating that intravenous injection of PEG-GCV-lipo was more suitable for a long circulation than intraperitoneal injection. Therefore, intravenous injection of GCV solution that has been used clinically, and PEG-GCV-lipo were used in subsequent experiments.

Table 3
Pharmacokinetics parameters after intravenous or intraperitoneal injections of GCV solution and PEG-GCV-lipo at a dose of 10 mg/kg in ddY mice

Formulation	Route of administration	$AUC^a_{0-12\ h}$ (μg h ml^{-1})	CL^b (ml h^{-1})	$t^c_{1/2}$ (h)
GCV solution	i.v.	4.8±0.7	14.9±5.7	0.4
	i.p.	4.6±0.9	45.0±8.5	0.5
PEG-GCV-lipo	i.v.	173.2±13.7	1.2±0.1	5.3
	i.p.	143.4±21.9	1.4±0.2	8.4

[a]AUC: area under the curve.
[b]CL: clearance.
[c]$t_{1/2}$: terminal half-life (mean).
Each value represents the mean±S.D. (N=4).

3.6. Biodistribution in nude mice bearing KB tumor xenografts

The tissue distribution of PEG-GCV-lipo after intravenous injection was examined in nude mice bearing KB tumor xenografts (Fig. 3). For the comparison, GCV solution, which has been used clinically, was used. The majority of liposomes accumulated in the spleen or liver rather than in the tumor, and GCV solution was scarcely accumulated in each tissue. In serum and all tissue administered PEG-GCV-lipo, GCV concentration was higher at 12 h than at 24 h after injection. The GCV concentration of PEG-GCV-lipo in the serum was 3.4 μg/ml 24 h after injection, but that of GCV solution was not detected. In the liver, spleen and lung, GCV concentration was significantly higher from PEG-GCV-lipo than GCV solution 24 h after injection; however, in the heart, GCV was hardly detected 24 h after PEG-GCV-lipo administration. In tumors, GCV concentration was higher from PEG-GCV-lipo than GCV solution.

3.7. In vivo efficacy in GCV/HSV-TK suicide gene therapy

The efficacy of PEG-GCV-lipo after intravenous injection was evaluated in KB tumor xenografts by GCV/HSV-TK gene

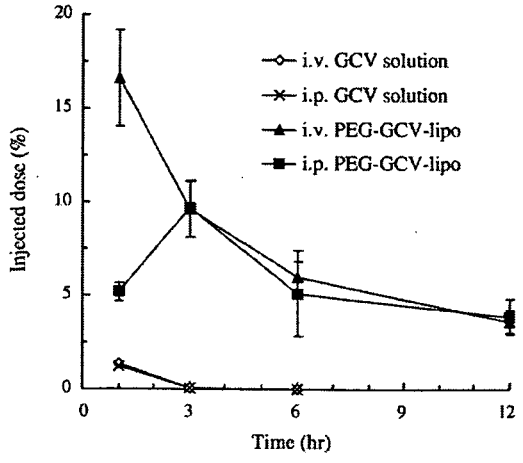

Fig. 2. GCV injected dose (%) in serum-time curves of GCV solution and PEG-GCV-lipo following intravenous or intraperitoneal injections at a dose of 10 mg GCV/kg in ddY mice. Data points indicate the mean±S.D. (N=4).

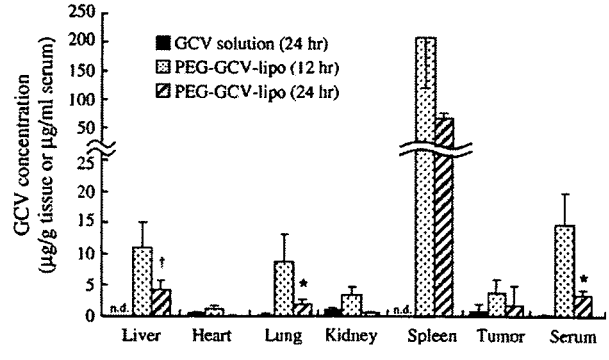

Fig. 3. Tissue distribution of GCV 12 or 24 h after intravenous injection of PEG-GCV-lipo, and 24 h after intravenous injection of GCV solution at a single dose of 25 mg GCV/kg into KB tumor-bearing BALB/c nude mice. Data indicate the mean±S.D. (N=3–4). n.d.; not detected, *P<0.05 compared with GCV solution (24 h), †P<0.05 compared with PEG-GCV-lipo (12 h).

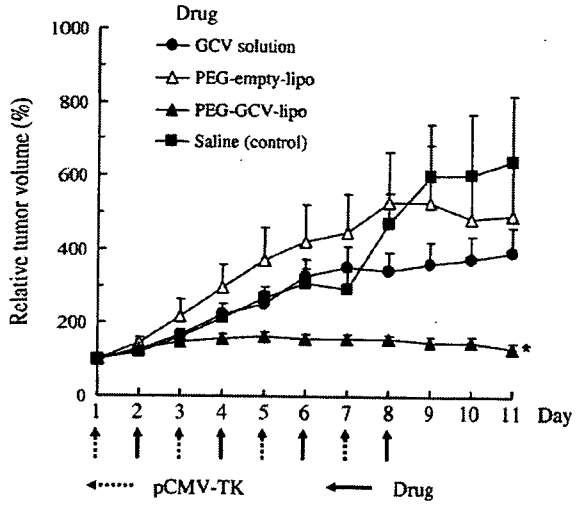

Fig. 4. In vivo effects of PEG-GCV-lipo on KB tumors expressing HSV-TK. Twelve days after subcutaneous inoculation of KB cells in BALB/c nude mice, complexes of pCMV-TK with gene vector were injected directly into the tumor four times (days 1, 3, 5 and 7). GCV solution, saline and PEG-empty-lipo or PEG-GCV-lipo were administered following daily intravenous injection the day after the injection of complexes. The dose of GCV solution and long-circulating liposome-encapsulated GCV (PEG-GCV-lipo) was 25 mg GCV/kg. Data points indicate the mean±S.E. (N=3–4). *P<0.05, comparing PEG-GCV-lipo with GCV solution at day 11.

therapy. After mice were given a direct injection of pCMV-TK with nanoparticles at 1, 3, 5 and 7 days, they were treated intravenously with PEG-empty-lipo, PEG-GCV-lipo, GCV solution and saline at 2, 4, 6 and 8 days. Treatment with PEG-GCV-lipo inhibited tumor growth and relative tumor volume was not increased after injection (Fig. 4). At 11 days, PEG-GCV-lipo was significantly 3-fold more effective than GCV solution in inhibiting tumor growth (P<0.05) and produced durable complete tumor remissions.

4. Discussion

The therapeutic efficacy of HSV-TK/GCV gene therapy depended on transfection of the TK gene, and the metabolization of available GCV. The eradication of TK-expressing tumors with GCV is important. For this purpose, we developed long-circulating liposome-encapsulated GCV. We demonstrated that GCV encapsulated in liposomes exhibited sustained release, which enhanced cytotoxicity in suicide gene therapy in vitro and in vivo.

GCV is water-soluble (dissolved up to 2.5 mg/ml in water). Liposomes can incorporate both water-soluble and insoluble drugs [19]; however, the entrapment efficiency of water-soluble substances into liposomes is low because liposomes have a small volume of entrapped aqueous space per mole of lipid [20]. We used the freeze–thawing method to prepare liposome-encapsulated GCV. The thaw temperature in the preparation of GCV-lipo did not change the particle size, but exhibited significantly high entrapment efficiency of GCV at 4 °C (Table 1). It was reported that the use of cold air to thaw liposomes was effective for increasing internal volume [21]; thus, thawing at 4 °C was a suitable condition to increase entrapment efficiency.

The addition of OA and SA as a component of liposomes increased the entrapment efficiency of GCV in liposomes. OA and SA are negatively and positively charged lipids, respectively. GCV is an amphoteric drug. The pK_a values for GCV are 2.2 and 9.4, so that GCV is un-ionized at pH 2.2–9.4. Ionized acyclovir, analogized GCV, was active to interact with both positively and negatively charged components of the liposomes by electrostatic interaction and increased entrapment [22]. Similar to acyclovir, partially ionized GCV might trigger interaction with positively and negatively charged lipids.

The IC_{50} values of PEG-GCV-lipo in HeLa cells were higher than non-PEGylated liposomes although they showed similar release profiles. This is probably related to the steric effect of the PEG chain, which may delay cell internalization of the drug [23]. Similar to this study, PEGylated liposome-encapsulated docetaxel exhibited lower cytotoxicity than non-PEGylated liposomes [24].

Interestingly, intraperitoneal injection of PEG-GCV-lipo exhibited a long circulation as well as intravenous injection (Fig. 2). This result corresponded with a report that PEG-coating liposomes after intraperitoneal injection can reach the blood stream and showed similar AUC values following intravenous administration [25]. GCV with PEG-GCV-lipo 24 h after intravenous injection was still remained in blood stream and distributed to tissues including tumor (Fig. 3). This suggested that PEG-GCV-lipo might accumulate in the tumor by EPR effect. Hydrophilic PEG chains exposed to aqueous surroundings may prevent the adsorption of blood proteins onto the liposome surface and prevent them from being cleared through the reticuloendothelial system [26].

Actually, in the suicide gene therapy schedules reported, GCV was administered at a high dose (~100 mg/kg) and frequency (e.g. twice daily, over 5 days) [7,9,10,14]. In this study, we administered PEG-GCV-lipo (25 mg/kg) once daily and 4 times (Fig. 4). The relative tumor volume of injected PEG-GCV-lipo was not changed throughout this experiment; therefore, this finding indicates that the administered dose and time of GCV could be decreased by using PEG-GCV-lipo.

In this study, we prepared PEGylated GCV-lipo using an optimized formulation with EPC:Chol:SA=5:5:1 (molar ratio) and the freeze–thawing method with thawing at 4 °C. In vitro, we demonstrated that the cytotoxicity of GCV-lipo and PEG-GCV-lipo was similar to those of GCV solution in HeLa-TK cells. In vivo, intravenously administered PEG-GCV-lipo significantly inhibited the tumor growth of KB xenografts expressing HSV-TK. These findings indicated that PEG-GCV-lipo, a long-circulating drug carrier, is a new approach to enhance the cytotoxic effect of suicide gene therapy.

Acknowledgments

We thank Mr. Atsushi Yamada and Mr. Takashi Yoshizawa for their assistance in the experimental work. We are also grateful to Mr. Takayuki Agatsuma, Ms. Yoshie Terakado and Ms. Satomi Mizuno for their technical assistance.

References

[1] Y. Gunji, T. Ochiai, H. Shimada, H. Matsubara, Gene therapy for cancer, Surg. Today 30 (2000) 967–973.

[2] C.J. Springer, I. Niculescu-Duvaz, Prodrug-activating systems in suicide gene therapy, J. Clin. Invest. 105 (2000) 1161–1167.

[3] C. Fillat, M. Carrio, A. Cascante, B. Sangro, Suicide gene therapy mediated by the Herpes Simplex virus thymidine kinase gene/ganciclovir system: fifteen years of application, Curr. Gene Ther. 3 (2003) 13–26.

[4] D.F. Smee, Interaction of 9-(1,3-dihydroxy-2-propoxymethyl)guanine with cytosol and mitochondrial deoxyguanosine kinases: possible role in anti-cytomegalovirus activity, Mol. Cell. Biochem. 69 (1985) 75–81.

[5] E.C. Mar, J.F. Chiou, Y.C. Cheng, E.S. Huang, Inhibition of cellular DNA polymerase alpha and human cytomegalovirus-induced DNA polymerase by the triphosphates of 9-(2-hydroxyethoxymethyl)guanine and 9-(1,3-dihydroxy-2-propoxymethyl)guanine, J. Virol. 53 (1985) 776–780.

[6] Y. Hattori, Y. Maitani, Folate-linked nanoparticle-mediated suicide gene therapy in human prostate cancer and nasopharyngeal cancer with herpes simplex virus thymidine kinase, Cancer Gene Ther. 12 (2005) 796–809.

[7] K. Hayashi, T. Hayashi, H.D. Sun, Y. Takeda, Contribution of a combination of ponicidin and acyclovir/ganciclovir to the antitumor efficacy of the herpes simplex virus thymidine kinase gene therapy system, Hum. Gene Ther. 13 (2002) 415–423.

[8] S.H. Yang, T.K. Oh, S.T. Kim, Increased anti-tumor effect by a combination of HSV thymidine kinase suicide gene therapy and interferon-gamma/GM-CSF cytokine gene therapy in CT26 tumor model, J. Korean Med. Sci. 20 (2005) 932–937.

[9] E. Nishihara, Y. Nagayama, F. Mawatari, K. Tanaka, H. Namba, M. Niwa, S. Yamashita, Retrovirus-mediated herpes simplex virus thymidine kinase gene transduction renders human thyroid carcinoma cell lines sensitive to ganciclovir and radiation in vitro and in vivo, Endocrinology 138 (1997) 4577–4583.

[10] C. Engelmann, Y. Panis, J. Bolard, B. Diquet, M. Fabre, H. Nagy, O. Soubrane, D. Houssin, D. Klatzmann, Liposomal encapsulation of ganciclovir enhances the efficacy of herpes simplex virus type 1 thymidine kinase suicide gene therapy against hepatic tumors in rats, Hum. Gene Ther. 10 (1999) 1545–1551.

[11] F. Miura, S. Moriuchi, M. Maeda, A. Sano, M. Maruno, A.M. Tsanaclis, R. Marino Jr., J.C. Glorioso, T. Yoshimine, Sustained release of low-dose ganciclovir from a silicone formulation prolonged the survival of rats with gliosarcomas under herpes simplex virus thymidine kinase suicide gene therapy, Gene Ther. 9 (2002) 1653–1658.

[12] C. Giannavola, C. Bucolo, A. Maltese, D. Paolino, M.A. Vandelli, G. Puglisi, V.H. Lee, M. Fresta, Influence of preparation conditions on acyclovir-loaded poly-d,l-lactic acid nanospheres and effect of PEG coating on ocular drug bioavailability, Pharm. Res. 20 (2003) 584–590.

[13] Y. Matsumura, H. Maeda, A new concept for macromolecular therapeutics in cancer chemotherapy: mechanism of tumoritropic accumulation of proteins and the antitumor agent smancs, Cancer Res. 46 (1986) 6387–6392.

[14] P.S. Uster, T.M. Allen, B.E. Daniel, C.J. Mendez, M.S. Newman, G.Z. Zhu, Insertion of poly(ethylene glycol) derivatized phospholipid into pre-formed liposomes results in prolonged in vivo circulation time, FEBS Lett. 386 (1996) 243–246.

[15] R. Boulieu, N. Bleyzac, S. Ferry, High-performance liquid chromatographic determination of ganciclovir in plasma, J. Chromatogr., Biomed. Appl. 567 (1991) 480–484.

[16] S. Takemoto, K. Yamaoka, M. Nishikawa, Y. Takakura, Histogram analysis of pharmacokinetic parameters by bootstrap resampling from one-point data in animal experiments, Drug Metab. Pharmacokinet. 21 (2006) 458–464.

[17] K. Hayashi, T. Hayashi, N. Morita, Mechanism of action of the antiherpesvirus biflavone ginkgetin, Antimicrob. Agents Chemother. 36 (1992) 1890–1893.

[18] Y. Hattori, H. Kubo, K. Higashiyama, Y. Maitani, Folate-linked nanoparticles formed with DNA complexes in sodium chloride solution enhance transfection efficiency, J. Biomed. Nanotechnol. 1 (2005) 176–184.

[19] P. Crosasso, M. Ceruti, P. Brusa, S. Arpicco, F. Dosio, L. Cattel, Preparation, characterization and properties of sterically stabilized paclitaxel-containing liposomes, J. Control. Release 63 (2000) 19–30.

[20] P.A. Monnard, T. Oberholzer, P. Luisi, Entrapment of nucleic acids in liposomes, Biochim. Biophys. Acta 1329 (1997) 39–50.

[21] K. Anzai, M. Yoshida, Y. Kirino, Change in intravesicular volume of liposomes by freeze-thaw treatment as studied by the ESR stopped-flow technique, Biochim. Biophys. Acta 1021 (1990) 21–26.

[22] S.L. Law, H.Y. Hung, Properties of acyclovir-containing liposomes for potential ocular delivery, Int. J. Pharm. 161 (1998) 253–259.

[23] M.C. Woodle, Surface-modified liposomes: assessment and characterization for increased stability and prolonged blood circulation, Chem. Phys. Lipids 64 (1993) 249–262.

[24] M.L. Immordino, P. Brusa, S. Arpicco, B. Stella, F. Dosio, L. Cattel, Preparation, characterization, cytotoxicity and pharmacokinetics of liposomes containing docetaxel, J. Control. Release 91 (2003) 417–429.

[25] T.M. Allen, C.B. Hansen, L.S. Guo, Subcutaneous administration of liposomes: a comparison with the intravenous and intraperitoneal routes of injection, Biochim. Biophys. Acta 1150 (1993) 9–16.

[26] K. Maruyama, T. Yuda, A. Okamoto, S. Kojima, A. Suginaka, M. Iwatsuru, Prolonged circulation time in vivo of large unilamellar liposomes composed of distearoyl phosphatidylcholine and cholesterol containing amphipathic poly(ethylene glycol), Biochim. Biophys. Acta 1128 (1992) 44–49.

Non-viral delivery of the connexin 43 gene with histone deacetylase inhibitor to human nasopharyngeal tumor cells enhances gene expression and inhibits *in vivo* tumor growth

YOSHIYUKI HATTORI, MASAYOSHI FUKUSHIMA and YOSHIE MAITANI

Institute of Medicinal Chemistry, Hoshi University, Shinagawa-ku, Tokyo 142-8501, Japan

Abstract. Dysregulation of connexin expression is believed to have a role in carcinogenesis, because levels of connexin are reduced in various tumors. We examined the role of connexin 43 (Cx43) alone and combined with a histone deactylase (HDAC) inhibitor in tumor growth inhibition. The transfection of Cx43 plasmid DNA (pCMV-Cx43) into human nasopharyngeal cancer KB cells using folate-linked nanoparticles induced inhibition of cell growth. Cx43 induced a tumor suppressive effect via a gap junctional intercellular communication-independent mechanism. The transfection of pCMV-Cx43 along with an HDAC inhibitor, 4-phenylbutyrate (4-PB), enhanced Cx43 expression greatly *in vitro*, and inhibited significantly the tumor growth of KB cells and xenografts compared with that of pCMV-Cx43 alone. 4-PB induced increased expression of genes of DNA damage checkpoints and of apoptosis via the down-regulation of anti-apoptotic bcl-2 mRNA expression and up-regulation of the activity of the apoptosis-associated enzyme caspase-3/7. Thus, the amplified Cx43 expression by an antitumor agent, an HDAC inhibitor, may have great potential as a growth inhibitor for nasopharyngeal tumors.

Introduction

Deregulation of connexin (Cx) expression is believed to play a part in carcinogenesis (1). Cx proteins have an essential role in gap junction intercellular communication (GJIC), which is often impaired among tumor cells and between tumor cells and surrounding normal cells. Connexin 43 (Cx43) is a tumor-suppressor (2), and its expression is reduced in various tumors (3-10). Forced expression of the Cx43 gene in several Cx43-deficient tumor cell lines attenuated their malignant phenotype (8,11). However, a truncated Cx43 not forming gap junctions, also inhibited tumor growth (12). Thus, the mechanisms by which the Cx43 gene inhibits tumor growth remain unclear. Regarding tumor gene therapy using the Cx gene, there are many reports about co-administration of the herpes simplex thymidine kinase (HSV-tk) gene (13) or a chemotherapeutic agent (14,15). Enforced expression of Cx resulted in a dramatic suppression of tumor growth when Cx gene-transfected tumor cells were implanted into mice (1). However, the application of Cx gene delivery *in vivo* by direct injection into tumor-bearing mice with a vector has not been reported except for injection of the Cx26 gene with an adenoviral vector (16). One major obstacle to applications *in vivo* is poor transgene expression, therefore, a transfer system including an efficient vector for the Cx gene is required to strongly induce gene expression *in vivo*.

Histone deacetylase (HDAC) inhibitors such as sodium butyrate (SB), 4-phenylbutyrate (4-PB) and trichostatin A (TSA) cause cell-cycle arrest in the G_1 and/or G_2 phase and induce differentiation and/or apoptosis in a variety of cell types (17). Inhibition of HDAC activity induces the transcriptional activation of certain genes, such as that for the cyclin-dependent kinase inhibitor p21, which are thought to suppress tumor growth and prevent cell cycle progression (18,19). Several HDAC inhibitors inhibit tumor growth in animal models with little toxicity in non-tumor cells (20). Therefore, HDAC inhibitors are a new class of antitumor agent being evaluated in clinical trials. HDAC inhibitors also possess the capacity to enhance the expression of a wide variety of transiently transfected transgenes in tumors both *in vitro* and *in vivo* through their effect on the acetylation of histones (19,21). Combining of p53 gene therapy with an HDAC inhibitor, FR901228 or SB, enhanced therapeutic efficacy *in vitro* (22) and *in vivo* (23). The introduction of both the HSV-tk gene and FR901228 into melanoma xenografts enhanced the antitumor effect (24). However, the effect of transfection of the Cx gene combined with an HDAC inhibitor has not been reported.

The development of non-viral and tumor-selective delivery vectors for gene transfer *in vivo* is necessary for the clinical application of therapeutic genes. Folate receptor (FR) has been found to be overexpressed in a wide range of tumors (25). We previously reported that folate-linked nanoparticles (NP-F) could efficiently deliver DNA into human nasopharyngeal cancer KB cells, which overexpressed FR (26,27).

Correspondence to: Dr Yoshiyuki Hattori, Institute of Medicinal Chemistry, Hoshi University, Shinagawa-ku, Tokyo 142-8501, Japan
E-mail: yhattori@hoshi.ac.jp

Key words: connexin 43, histone deacetylase inhibitor, nasopharyngeal cancer, 4-phenylbutyrate, gene therapy, folate-linked nanoparticle, trans-fection, gap junction, apoptosis

Therefore, we used NP-F as a DNA transfection vector for cancer gene therapy.

In the present study, we investigated whether the transfection of plasmid DNA (pCMV-Cx43) coding for the Cx43 gene by NP-F combined with an HDAC inhibitor induced inhibition of KB cell growth. A novel combination of pCMV-Cx43 and an HDAC inhibitor, 4-PB enhanced the expression of Cx43 protein and induced significantly greater growth inhibition in KB cells and the tumor xenografts compared with pCMV-Cx43 alone. This combination increased apoptosis via down-regulation of bcl-2 mRNA expression and up-regulation of caspase-3/7 activity.

Materials and methods

Materials. SB and 4-PB were purchased from Wako Pure Chemicals (Osaka, Japan). TSA was supplied by Sigma Chemical Co. (St. Louis, MO, USA). 1,1'-Dioctadecyl-3, 3, 3', 3'-tetramethylindocarbocyamine perchlorate (DiI) was obtained from Lambda Probes & Diagnostics (Graz, Austria). Calcein-AM was purchased from Dojindo (Kumamoto, Japan). The Pica gene luciferase assay kit was obtained from Toyo Ink Mfg. Co. Ltd. (Tokyo, Japan). Bicinchonic acid (BCA) protein assay reagent was purchased from Pierce (Rockford, IL, USA). All reagents were of analytical grade. All other chemicals used were of reagent grade. Folate-deficient RPMI-1640 medium and fetal bovine serum were purchased from Life Technologies, Inc. (Grand Island, NY, USA).

Preparation of plasmid DNA. In the construction of the plasmid pCMV-Cx43 encoding the Cx43 gene under the control of the CMV promoter, the Cx43 and CMV promoter DNAs were amplified as described previously (28). After the Cx43 DNA amplification, this DNA was subcloned into an *Nco*I/*Xba*I-digested pGL3-control (Promega, Madison, WI, USA). Subsequently, the amplified CMV promoter DNA was subcloned into the *Hin*dIII and *Kpn*I restriction sites of the above plasmid.

In the construction of the plasmid pCMV-Cx43-EGFP, EGFP was fused in frame to the carboxyl terminus of Cx43. The DNA coding for EGFP was amplified by PCR using pEGFP-C1 (Clontech, CA, USA) as a template and the following EGFP-specific primers: EGFP forward primer (5'-TTGGCGCCGTGGGCAAGGGCGAGGAGCTG-3'), EGFP reverse primer (5'-TTTCTAGATTAGGACTTGTACAGCTCCTCC-3'). The forward primer contained a *Nar*I restriction site (underlined). The reverse primer contained an *Xba*I restriction site (underlined). The cDNA encoding bp 1-1146 of human Cx43 was amplified by PCR using the following Cx43-specific primers: Cx43 forward primer (5'-GCAAGCTTaccATGGGTGACTGGAGCGCCT-3'), Cx43 reverse primer (5'-ATGGCGCCGATCTCCAGGTCATCAGGCC-3'). The forward primer contained a 3-bp optimal Kozak sequence (in lower case letters) together with a *Hin*dIII restriction site (underlined). The reverse primer coded for bp 1129-1146 of Cx43 with a *Nar*I restriction site (underlined). After the DNA amplification of EGFP, this DNA was digested with *Nar*I and *Xba*I and was ligated into a *Nar*I and *Xba*I-digested pGL3-enhancer (Promega). Subsequently, the amplified PCR fragment of Cx43 was cloned into the *Hin*dIII and *Nar*I-restriction sites of the above plasmid, and then the CMV promoter DNA was subcloned into the *Hin*dIII and *Kpn*I-restriction sites as described above.

In the construction of the plasmid pCMV-luc encoding the luciferase gene under the control of the CMV promoter, the CMV promoter DNA was subcloned into the *Hin*dIII and *Kpn*I restriction sites of pGL3-enhancer. pGL3-basic encoding the luciferase gene without promoter was obtained from Promega and used as a control plasmid. A protein-free preparation of these plasmids was purified following alkaline lysis using maxiprep columns (Qiagen, Hilden, Germany).

Preparation of folate-linked nanoparticles. Cholesteryl-3ß-carboxyamidoethylene-N-hydroxyethylamine (OH-Chol) was synthesized as previously reported (27). NP-F as a gene transfection reagent was prepared with lipids [OH-Chol: Tween-80 (NOF Co. Ltd., Tokyo, Japan): folate-polyethylene glycol-distearoylphosphatidylethanolamine (mean molecular weight of PEG: 2,000 kDa) = 94:5:1, molar ratio = 10:1.3:0.65 weight] in 10 ml of water using a modified ethanol injection method as described previously (27).

Cell culture. KB cells were from the Cell Resource Center for Biomedical Research, Tohoku University (Miyagi, Japan). Prostate cancer LNCaP cells were supplied by the Department of Urology, Keio University Hospital (Tokyo, Japan). All the cell lines used in this study were grown in a folate-deficient RPMI-1640 medium supplemented with 10% heat-inactivated fetal bovine serum and kanamycin (100 μg/ml) at 37°C in a 5% CO_2 humidified atmosphere.

In vitro transfection. Cell cultures were prepared by plating cells in a 35-mm culture dish 24 h prior to each experiment. Based on preliminary experiments *in vitro*, the optimized charge ratio (+/-) of cationic lipid to DNA was determined as 3:1 (27). The NP-F and plasmid DNA complex (NP-F nanoplex) at a charge ratio (+/-) of cationic lipid to DNA of 3/1 was formed by addition of NP to 2 μg of plasmid DNA in 50 mM NaCl with gentle shaking and left at room temperature for 10 min. The NP-F nanoplex was diluted in 1 ml of medium supplemented with 10% serum and then incubated with cells for 24 h. For the co-introduction of the HDAC inhibitor, the NP-F nanoplex was diluted in the medium containing the HDAC inhibitor to the concentration indicated in the figure legends.

In vitro cell growth. KB cells were seeded separately at a density of $1x10^4$ cells per well in 96-well plates and maintained for 24 h before transfection in RPMI medium supplemented with 10% serum. The cells at 30% confluence in the well were transfected with the NP-F nanoplexes using 0.2 μg of pCMV-Cx43 or pGL3-basic in the presence or absence of the HDAC inhibitor and incubated for 48 h. The cell number was determined with a WST-8 assay (Dojindo Laboratories).

Immunoblotting. KB cells were seeded in a 35-mm culture dish and incubated overnight. The cells at 30% confluency were transfected with pCMV-Cx43 or pGL3-basic in the presence or absence of the HDAC inhibitor and then incubated for 24 h. The cells were suspended in lysis buffer [1%

Triton X-100 in phosphate-buffered saline pH 7.4 (PBS)], and then centrifuged at 15,000 rpm for 10 min. The supernatants (10 μg protein) were resolved on a 12% sodium dodecyl sulphate-polyacrylamide gel by electrophoresis (SDS-PAGE) and transferred to a polyvinylidene difluoride (PVDF) membrane (FluoroTrans® W, PALL Gelman Laboratory, Ann Arbor, MI, USA). Expression of the Cx43 protein was identified using a specific rabbit antiserum (Sigma) and acetylated histone H3 was detected by rabbit anti-human acetyl histone H3 antibody (Sigma). The goat anti-rabbit IgG peroxidase conjugate (Santa Cruz Biotechnology, Inc., Santa Cruz, CA, USA) was used as secondary antibody. These proteins were detected with peroxidase-induced chemiluminescence (Super Signal West Pico Chemiluminescent Substrate, Pierce).

RNA isolation and RT-PCR. KB cells were seeded in a 35-mm culture dish and incubated overnight. The cells at 30% confluency were transfected with pCMV-Cx43 or pGL3-basic in the presence or absence of 1 μM TSA, 1 mM SB or 1 mM 4-PB, and then incubated for 24 h. Total RNA was isolated from the cells using NucleoSpin RNA II (Macherey-Nagel, Germany). First-strand cDNA was synthesized from 5 μg of total RNA as previously described (28). For RT-PCR, the 25-μl reaction volume contained the following: 1 μl of synthesized cDNA, 10 pmol of each specific primer pair, and 0.25 units of Ex Taq DNA polymerase (Takara Shuzo Co., Ltd) with a PCR buffer containing 1.5 mM $MgCl_2$ and 0.2 mM of each dNTP. The profile of PCR amplification consisted of denaturation at 94˚C for 0.5 min, primer annealing at 58˚C for 0.5 min, and elongation at 72˚C for 1 min for 25 cycles. For the amplification of human Cx43, the primers Cx43-FW, 5'-CTC ATGTGTTCTATGTGATG-3', and Cx43-RW, 5'-ATTGCG GCAAGAAGAATTGT-3', were used. For the amplification of human bcl-2, the primers bcl-2-FW, 5'-TGGAGAGCGTC AACCGGGAG-3', and bcl-2-RW, 5'-CCGTACAGTTCCAC AAAGGC-3', were used. For the amplification of the housekeeping gene ß-actin, the primers ß-actin-FW, 5'-ACCCACA CTGTGCCCATCTA-3', and ß-actin-RW, 5'-CTGCTTGCT GATCCACATCT-3', were used. PCRs of Cx43, bcl-2 and ß-actin were performed at the same cycle run for all samples. The PCR products for Cx43, bcl-2 and ß-actin were analyzed by 1.5% agarose gel electrophoresis in a Tris-borate-EDTA (TBE) buffer. The products were visualized by ethidium bromide staining.

Real-time PCR was performed on the corresponding cDNA synthesized from each sample described above. The optimized settings were transferred to the real-time PCR protocol with the iCycler MyiQ detection system (Bio-Rad Laboratories, Hercules, CA, USA) and SYBR-Green I assay (iQ™ SYBR-Green Supermix, Bio-Rad Laboratories) was used for quantification. Samples were run in triplicate and the expression levels of Cx43 and bcl-2 mRNA were normalized to the amount of ß-actin in the same sample.

cDNA array. KB cells were seeded in a 35-mm culture dish and incubated overnight. The cells at 30% confluency were transfected with pGL3-basic or pCMV-Cx43 in the presence or absence of 1 μM TSA or 1 mM 4-PB. After 24 h of incubation, total RNA was isolated from the cells as described above. A non-radioactive human cell cycle gene array (GEArray Q series human cell cycle gene assay, Super Array Inc., MD, USA) was used to analyze the gene expression profile of the cell cycle, DNA damage checkpoint and ATM pathway. Briefly, 5 μg of total RNA was used as a template to produce biotinylated cDNA probes. RNA was reverse-transcribed using gene-specific primers with biotin-16-dUTP. Biotinylated cDNA probes were denatured and hybridized to cell cycle gene-specific cDNA fragments spotted on membranes. The GEArray membranes were then washed and blocked with GEA blocking solution, and incubated with alkaline phosphatase-conjugated streptavidin. The hybridized biotinylated probes on the membrane were detected by a chemiluminescent method using the alkaline phosphatase substrate, CDP-*Star*. The membranes were exposed to chemiluminescence film (Hyperfilm™ ECL™, Amersham Bioscience Corp., Piscataway, NJ, USA) for 10 sec. The results were analyzed using free ScanAlyze software (developed by Dr Michael Eisen), which converts a grayscale TIFF image of spots into numerical data (median pixel intensity), and then the gene expression profiles were compared using GEArray analyzer software (Super Array, Inc.). Each array comprised 96 marker genes in quadruplicate, 4 positive controls including ß-actin, glyceraldehyde-3-phosphate dehydrogenase (GAPDH), cyclophilin A (PPIA) and ribosomal protein L13a, and a negative control, the bacterial plasmid pUC18. Intensity was calculated from each array by subtracting the negative control from each spot and normalized against the housekeeping gene PPIA. Gene expression ratios from each experiment were calculated by using the average normalized intensities from each array.

Cell cycle analysis. KB cells were seeded in a 35-mm culture dish and incubated overnight. The cells at 30% confluency were transfected with pCMV-Cx43 or pGL3-basic in the presence or absence of 1 μM TSA, 1 mM SB or 1 mM 4-PB in medium. After 24 h of incubation, the cells were harvested with EDTA after a wash with ice-cold PBS. Detached cells were washed once with ice-cold PBS and gently suspended in PBS-EtOH (70%) and fixed overnight at 4˚C. For staining, the fixed cells were washed once in PBS and then resuspended in PBS with 50 μg/ml propidium iodide (PI) and 0.5% RNase A. After 30 min at 37˚C, the cells were processed for FACS analysis of the PI-fluorescence by a FACSCalibur flow cytometer (Becton-Dickinson, San Jose, CA) equipped with a 488-nm argon ion laser. Data for 10,000 fluorescent events were obtained by recording forward scatter (FSC), side scatter (SSC), and PI-fluorescence (585/42 nm).

Assesment of gap junctional intercellular communication. The FACS analysis of the GJIC reported by Robe *et al* (29) was modified. Briefly, cells grown in 35-mm dishes were labeled for 1-h incubation with either 5 μM calcein-AM or 5 μM DiI in the medium. The two labeled cells were mixed in equal proportions in 35-mm dishes and incubated for 24 h. Subsequently, pCMV-Cx43 or pGL3-basic was transfected with NP-F into the mixed cells in the presence or absence of 1 mM SB, 1 mM 4-PB or 1 μM TSA. After 24 h of incubation, the cells were trypsinized, washed in PBS and processed for a FACS analysis of the calcein-AM- and

DiI-fluorescences with a FACSCalibur flow cytometer as described above. Data for 10,000 fluorescent events were obtained by recording calcein-AM-fluorescence (530/30 nm) and DiI-fluorescence (585/42 nm).

Confocal microscopy. KB and LNCaP cells, respectively, were plated into 35-mm culture dishes. The cells at 30% confluency were transfected with pCMV-EGFP in the presence or absence of 1 μM TSA or 1 mM 4-PB by incubation for 24 h. Examinations were performed with a Radiance 2100 confocal laser scanning microscope (Bio-Rad Laboratories) as previously described (28). Cx43-EGFP was imaged using the 488-nm excitation line of an argon laser, and fluorescence emission was observed with a filter, HQ515/30.

Luciferase and caspase-3/7 activities. KB cells were seeded in a 35-mm culture dish and incubated overnight. The cells at 30% confluency were transfected with pGL3-basic or pCMV-Cx43 in the presence or absence of 1 μM TSA, 1 mM SB or 1 mM 4-PB by incubation for 24 h. For measuring caspase-3/7 activity, a homogenous assay (Caspase-Glo™ 3/7 assay, Promega, Madison, WI, USA) was performed as described in the assay instructions. Luciferase activity was measured using the luciferase assay system (Pica Gene, Toyo Ink Mfg. Co. Ltd., Tokyo, Japan) as previously reported (30).

Gene expression in vivo. To generate KB tumor xenografts, $1x10^7$ cells suspended in 50 μl of RPMI medium were inoculated subcutaneously into the flanks of male BALB/c nu/nu mice (7 weeks of age, Clea Japan, Inc., Tokyo, Japan). The tumor volume was calculated using the formula: tumor volume = 0.5 x a x b^2, where a and b are the larger and smaller diameters, respectively. Based on a preliminary experiment of gene expression induced by intratumoral injection, the optimized ratio of cationic lipid to DNA was determined as 1.5:1. For detection of luciferase gene expression in tumor, the nanoplex was formed by addition of NP-F (23.8 μl) to 10 μg of pCMV-luc with gentle shaking and standing at room temperature for 10 min. When the average volume of KB xenograft tumors reached approximately 600 mm^3, the NP-F nanoplexes of 10 μg of plasmid per tumor were directly injected into xenografts. Twenty-four hours after injections, the mice were injected with D-luciferin (potassium salt, Wako Pure Chemicals, Osaka, Japan) dissolved in PBS (125 mg/kg of body weight) into the peritoneal cavity and subsequently anesthetized by i.m. injection of 50 mg/kg body weight of pentobarbital (Nembutal, Dainippon Pharmaceutical Co., Ltd., Osaka, Japan). *In vivo* bioluminescence imaging was performed by using a NightOWL LB981 NC100 system (Berthold Technologies, Bad Wildbad, Germany). A gray scale body-surface reference image was collected using the NightOWL LB981 CCD camera. Photons emitted from luciferase within the mice were collected and integrated for a 2-min period. A pseudocolor luminescent image from blue (least intense) to red (most intense), representing the spatial distribution of the detected photons emitted within the mice, was generated using WinLight software (Berthold Technologies). The overlay of the real image and the luminescence representation allowed the localization and measurement of luminescence emitted from the tumor xenografts.

For detection of EGFP expression in tumor, the NP-F nanoplexes of 10 μg of pEGFP-C1 plasmid per tumor were directly injected into KB xenografts. Twenty-four hours after injections, tumors were removed for preparation of cryosections. The excised tumors were immediately frozen, sectioned at 20 μm thick and mounted. The expression of EGFP protein was observed using fluorescence microscopy.

Assessment of KB tumor growth. When the average volume of KB xenograft tumors reached 150 mm^3 (day 0), these mice were divided into four groups: group I, pGL3-basic (10 μg) as a control; group II, pCMV-Cx43 (10 μg); group III, pGL3-basic (10 μg) plus 1 mg 4-PB; and group IV, pCMV-Cx43 (10 μg) plus 1 mg 4-PB. Each experimental group consisted of 4 tumors. The NP-F nanoplexes at a charge ratio (+/-) of 1.5/1 of cationic lipid to DNA were formed as described in the above section. The nanoplexes of 10 μg of plasmid per tumor were directly injected into xenografts on days 0, 2 and 4. At 10 min after each DNA transfection, 20 μl of 50 mg/ml 4-PB dissolved in DMSO was directly injected into the xenografts. The tumor volume was measured at days 0, 2, 4, 6, 8, 11 and 13. At day 13, all mice were sacrificed, and the tumor weights were measured. Tumor volume and weight are shown as the mean ± SE and ± SD, respectively. The excised tumors were immediately frozen, sectioned 20-μm thick and mounted. The sections were stained with hematoxylin and pure eosin (Muto Pure Chemicals Co., Ltd., Tokyo, Japan) for histopathological examination.

Statistical analysis. The statistical significance of differences between mean values was determined using Welch's t-test. Multiple comparisons were performed with an analysis of variance followed by the Bonferroni/Dunn test. P-values <0.05 were considered significant.

Results

Amplification of Cx43 gene expression by HDAC inhibitors. In this study, we used NP-F for *in vitro* and *in vivo* DNA transfection into KB tumor. The *in vitro* transfection efficiency of pEGFP-C1 into KB cells by NP-F was ~20-30% at 30% confluency by flow cytometric analysis (data not shown). Commercially available transfection reagent Lipofectamine 2000 (Invitrogen Corp., Carlsbad, CA, USA) exhibited 40-50% transfection efficiency of the cells at 30% confluency, however, Lipofectamine 2000 is known to be cytotoxic and to induce expression of many apoptotic genes. In fact, the Lipofectamine 2000 significantly decreased cell viability after transfection into KB cells. Therefore, we decided to use NP-F for DNA transfection into KB cells.

To investigate whether the transfection of pCMV-Cx43 induced growth inhibition in the cells, we initially examined cell growth after transfection using a colorimetric viability assay. In this study, we used pGL3-basic as a control plasmid. Forty-eight hours after transfection, pCMV-Cx43 had a significant suppressive effect in KB cells (Fig. 1A).

Next, to induce the complete growth suppression of KB cells, we investigated whether the transfection of pCMV-Cx43 with an HDAC inhibitor, TSA, SB or 4-PB, enhanced the expression of Cx43. In a preliminary study, we observed

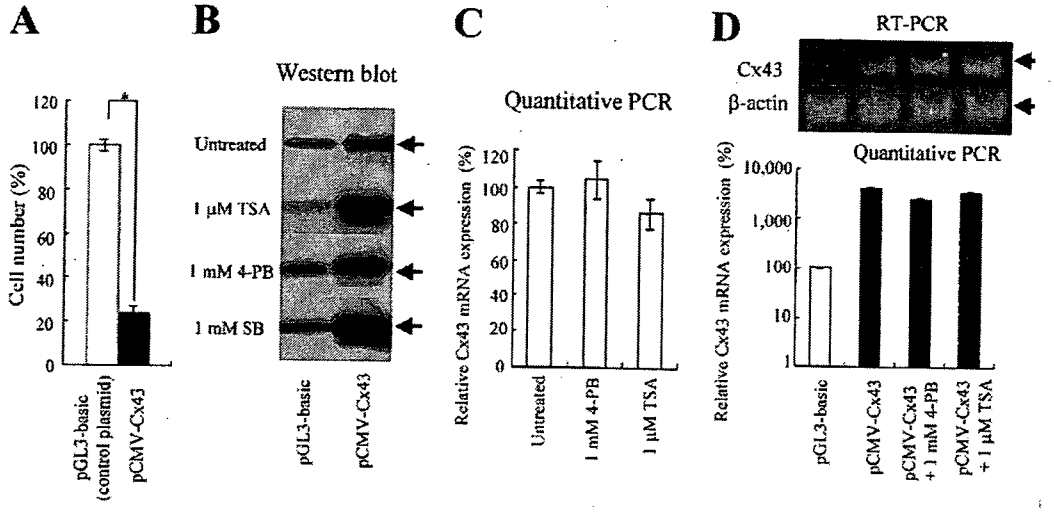

Figure 1. Effect on cell growth of expression of Cx43 (A) pGL3-basic was used as a control plasmid. The cells at 30% confluency were transfected with pCMV-Cx43 or pGL3-basic. Cell number was measured 48 h after transfection. Statistical significance of the data was evaluated with the Welch's t-test. *P<0.05, compared with pGL3-basic. Effect of HDAC inhibitors on the expression of Cx43 protein (B) and mRNA (C and D) in KB cells. The cells transfected with pCMV-Cx43 or pGL3-basic were exposed to 1 μM TSA, 1 mM 4-PB or 1 mM SB for 24 h (B and D). The cells were exposed to 1 μM TSA or 1 mM 4-PB for 24 h (C). Western blot (B) and quantitative PCR (C and D) and RT-PCR (D) analyses were performed 24 h after transfection. (B and C) The ß-actin housekeeping gene was used as the control. The relative amount of Cx43 mRNA in the cells was compared with a SYBR-Green I-based quantitative PCR analysis. The y-axis indicates Cx43 mRNA expression (%) of untreated (C) or pGL3-basic-transfected cells (D). The expression level of Cx43 mRNA was normalized to the amount of ß-actin in the same sample. Each result represents the mean ± SD (n=3).

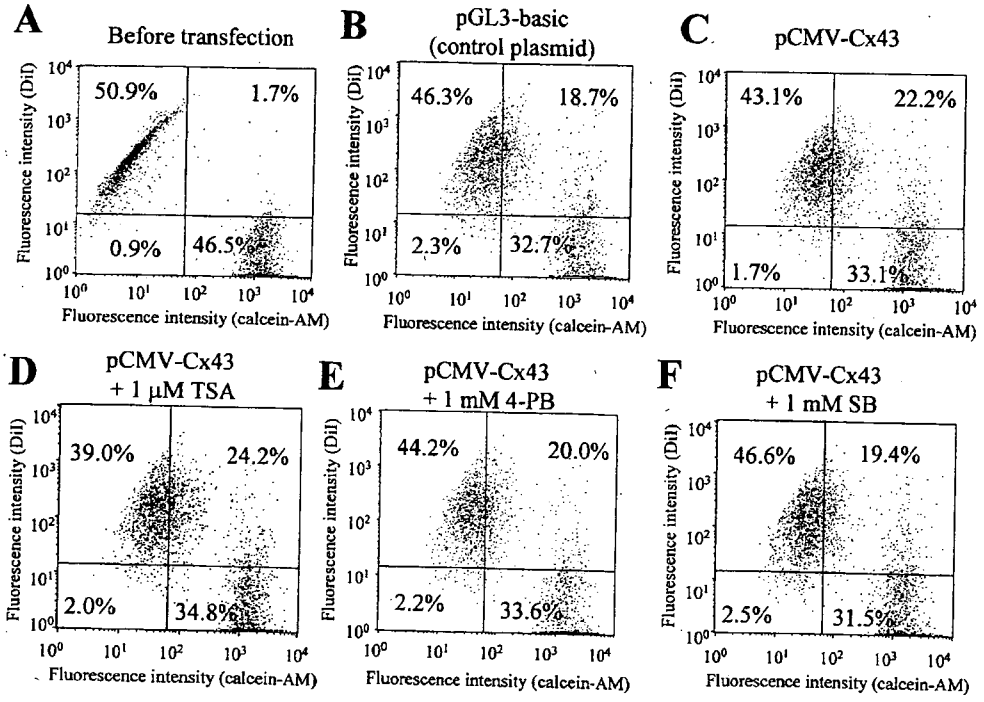

Figure 2. Gap junction-mediated transfer of fluorescent dyes in the presence and absence of HDAC inhibitors by FACS analysis. KB cells were pre-loaded with DiI and calcein-AM fluorescent probes. While DiI was retained in the preloaded cells, calcein-AM spread to DiI-positive cells, indicating gap junction-mediated transfer. The cells preloaded with DiI and calcein-AM were mixed in equal proportions, plated, and incubated for 24 h. The cells were transfected with pCMV-Cx43 or pGL3-basic in the presence or absence of 1 μM TSA, 1 mM SB or 1 mM 4-PB and incubated for another 24 h. Upper left quadrant, calcein-AM-loaded cells; lower right quadrant, DiI-tagged cells; upper right quadrant, DiI-tagged cells that have incorporated calcein-AM. Histogram of DiI-tagged and calcein-AM-loaded cells before co-incubation (A); pGL3-basic-transfected cells (B); pCMV-Cx43-transfected cells (C); pCMV-Cx43 plus TSA-transfected cells (D); pCMV-Cx43 plus 4-PB-transfected cells (E); pCMV-Cx43 plus SB-transfected cells (F).

the highest levels of Cx43 protein when the cells were co-introduced with 1 μM TSA, 1 mM SB and 1 mM 4-PB, respectively (data not shown). Therefore, in the subsequent experiment, we used these concentrations as optimal. The expression of endogenous Cx43 protein was detected moderately in KB cells (Fig. 1B, untreated cells transfected with

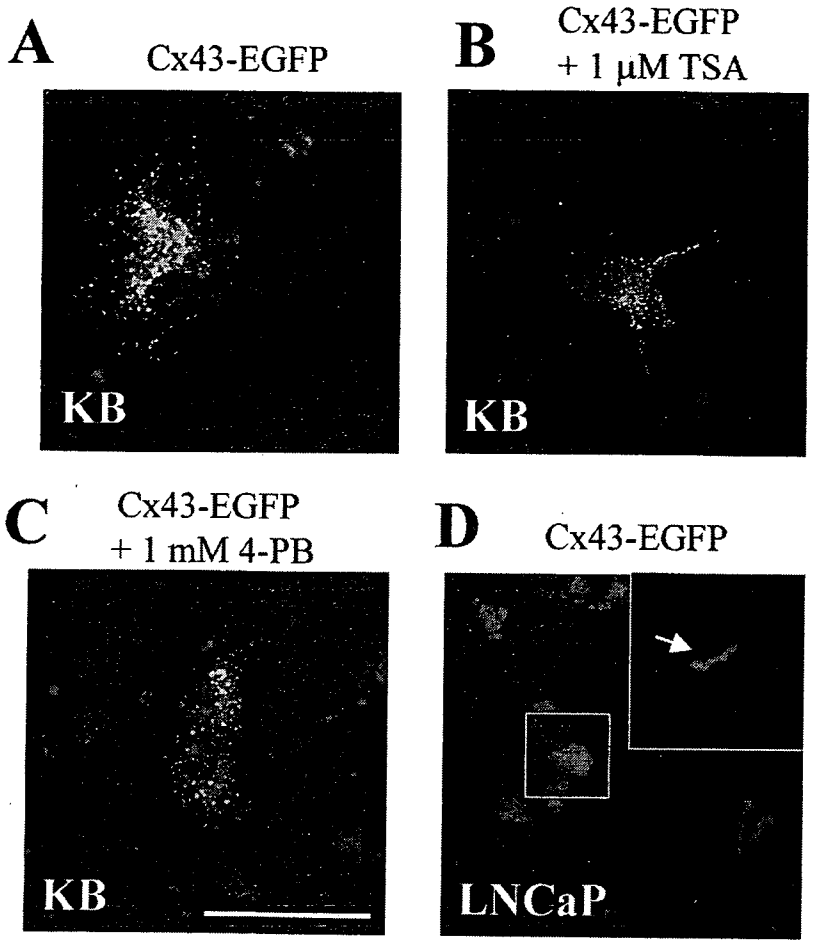

Figure 3. Localization of Cx43-EGFP in KB (A-C) and LNCaP cells (D). KB cells were transfected with pCMV-Cx43-EGFP in the absence (A) or presence of 1 μM TSA (B) or 1 mM 4-PB (C) for 24 h. LNCaP cells were transfected with pCMV-Cx43-EGFP for 24 h (D). The Cx43-EGFP was visualized by confocal microscopy (magnification x1,200). The red signals show the location of the nucleus, and the green signals, that of the Cx43-EGFP. Scale bar, 50 μm. Confocal images revealed that Cx43-EGFP was transported inefficiently to the cell surface and assembled into gap junctions in KB cells (A-C) while Cx43 was assembled more efficiently into gap junctions in LNCaP cells (D). Arrowheads indicate the junctional plaque.

pGL3-basic), and was weakly increased when the cells were treated with 4-PB or SB, but not TSA (Fig. 1B, pGL3-basic). When the cells were co-transfected with pCMV-Cx43 plus an HDAC inhibitor, the exogenous expression of Cx43 protein was strongly increased in the cells treated with each inhibitor, compared with those not treated with an inhibitor (Fig. 1B, pCMV-Cx43). Furthermore, we confirmed the increased expression of exogenous protein by HDAC inhibitors using pCMV-luc in the cells; the luciferase activity increased ~2- and 6-fold on treatment with TSA, and 4-PB and SB, respectively (data not shown). To confirm the effect on acetylation in histone by HDAC inhibitors, we analyzed the intracellular level of histone H3 acetylation using a specific antibody against acetylated histone H3. When KB cells were co-transfected with pCMV-Cx43 and TSA, SB or 4-PB, the increased Cx43 expression correlated with the increased acetylation of histone H3 (data not shown). The acetylation levels of histone H3 by HDAC inhibitors corresponded with a previous report (31).

To analyze the effect of HDAC inhibitors on the transcription of Cx43 mRNA, RT-PCR and quantitative PCR analyses were carried out in the cells transfected with pCMV-Cx43 in the presence or absence of HDAC inhibitors. As shown in Fig. 1C, endogenous Cx43 mRNA did not increase on treatment with 4-PB or TSA. In the cells transfected with pCMV-Cx43, the expression of Cx43 mRNA was ~40-fold higher than that with pGL3-basic (Fig. 1D). However, in the cells co-transfected with TSA or 4-PB, no amplification of Cx43 mRNA was observed compared to the cells without an HDAC inhibitor (Fig. 1D). Thus the amplified expression of Cx43 protein might result from an increase in Cx43 gene translation and/or from an indirect effect on stabilization of Cx43 protein by HDAC inhibitors.

Defective GJIC in KB tumor cells. To investigate whether the amplified expression of Cx43 protein by pCMV-Cx43 plus the HDAC inhibitor caused gap junctions to form, we assessed the transfer of calcein-AM, a cytoplasmic dye that crosses gap junctions, in a co-culture of calcein-AM-loaded cells and cells marked with DiI, a non-diffusible membrane fluorescent dye, by FACS analysis. pGL3-basic-transfected cells showed slight GJIC-mediated transfer of calcein-AM (18.7%) after 48-h culture (Fig. 2B), indicating that other kinds of Cx endogenously expressed in KB cells induced GJIC. The pCMV-Cx43-transfected cells did not exhibit a great increase

Table I. Differential expression of genes related to the cell cycle in KB cells on transfection of pCMV-Cx43 and/or treatment with HDAC inhibitors.

Gene name	pGL3-basic-transfected cells	pCMV-Cx43-transfected cells	pCMV-Cx43-transfected cells + 1 mM 4-PB	pCMV-Cx43-transfected cells + 1 μM TSA
G_1				
CDC7	17.1	58.2 (3.4)	77.0 (4.5)	81.2 (4.7)
cdk2	N.D	18.3	13.5	9.1
p16	12.3	79.1 (6.5)	70.6 (5.8)	41.7 (3.4)
Cks1 p9	42.6	84.1 (2.0)	74.6 (1.8)	26.3 (0.6)
Cullin2	N.D	60.9	66.2	48.8
Cullin3	N.D	22.2	10.2	30.1
Cullin4B	N.D	19.7	26.3	10.5
E2F-4	45.0	89.2 (2.0)	86.8 (1.9)	78.0 (1.7)
Nedd8	13.8	42.3 (3.1)	39.1 (2.8)	17.8 (1.3)
skp1	N.D	31.5	16.0	35.2
skp2	10.0	21.1 (2.1)	40.4 (4.1)	17.9 (1.8)
S				
Cyclin C	31.8	32.2 (1.0)	23.3 (0.7)	17.7 (0.6)
Cyclin G	42.2	67.8 (1.6)	79.5 (1.9)	72.7 (1.7)
Cyclin G2	16.6	15.2 (0.9)	27.6 (1.7)	17.5 (1.1)
CDC6	36.0	73.9 (2.1)	75.8 (2.1)	49.2 (1.4)
CDK7	17.1	58.2 (3.4)	77.0 (4.5)	81.2 (4.7)
MCM6	53.0	69.0 (1.3)	69.9 (1.3)	62.7 (1.2)
G_2				
Cyclin B	31.5	46.5 (1.5)	49.7 (1.6)	40.2 (1.3)
Cyclin B2	130.6	114.4 (0.9)	111.2 (0.9)	110.1 (0.8)
M				
cdk1	74.8	86.5 (1.2)	91.3 (1.2)	79.1 (1.1)
Cdc27	123.7	102.0 (0.8)	96.8 (0.8)	90.9 (0.7)
MAD2L1	N.D	14.4	11.1	3.9
PRC1	101.1	99.9 (1.0)	100.8 (1.0)	100.9 (1.0)
Rbx-1	12.6	36.0 (2.9)	15.8 (1.3)	5.7 (0.5)
DNA damage checkpoint and ATM pathway				
Apaf-1	97.9	102.6 (1.1)	105.1 (1.1)	99.3 (1.0)
ATM	73.1	84.5 (1.2)	87.3 (1.2)	79.9 (1.1)
chk1	18.9	58.8 (3.1)	61.4 (3.3)	40.3 (2.1)
MRE11A	N.D	27.8	28.5	13.3
MRE11B	N.D	19.3	48.2	26.7
nibrin	30.0	54.5 (1.8)	71.4 (2.4)	27.2 (0.9)
chk2	108.7	98.8 (0.9)	101.4 (0.9)	92.7 (0.9)
UBE1	23.1	70.6 (3.1)	73.4 (3.2)	56.4 (2.5)
E6-AP	N.D	23.2	14.8	11.7
SUMO-1	N.D	8.8	18.6	6.2
Control				
GAPDH	70.5	87.5 (1.2)	96.8 (1.4)	86.0 (1.2)
PPIA	100.0	100.0 (1.0)	100.0 (1.0)	100.0 (1.0)

This table shows the optical density of the spots in cDNA array. Median pixel intensity of each spot in cDNA array was calculated using ScanAlyze software, which is a program for DNA microarray imaging and extracts median pixel intensity from the image data of spots. The gene expression levels are shown as a percentage of the intensity compared with the corresponding internal control, PPIA. The ratio of gene expression between control cells and HDAC inhibitor-treated and/or pCMV-Cx43-transfected cells was assessed by the fold difference.

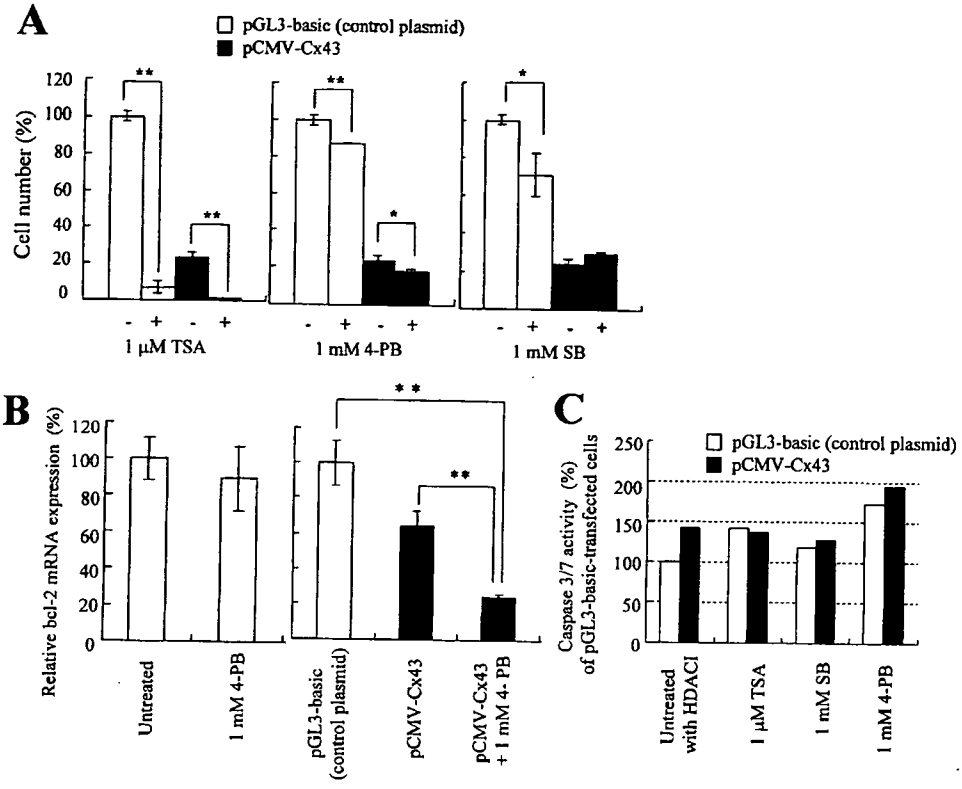

Figure 4. Effect of HDAC inhibitors on cytotoxicity in Cx43-transfected cells (A). KB cells were transfected with pCMV-Cx43 or pGL3-basic in the presence of 1 μM TSA, 1 mM SB or 1 mM 4-PB and incubated for 48 h. (B) Quantitative PCR analysis of bcl-2 mRNA expression in KB cells transfected with pCMV-Cx43 and/or 1 mM 4-PB. The y-axis indicates bcl-2 mRNA expression (%) of untreated or pGL3-basic-transfected cells. The expression level of bcl-2 mRNA was normalized to the amount of ß-actin in the same sample. Each result represents the mean ± SD (n=3). Statistical significance of the data was evaluated with Welch's t-test. **P<0.01, compared with pCMV-Cx43 plus 4-PB. (C) Effects of caspase-3/7 activities on Cx43-overexpressing KB cells by HDAC inhibitors. KB cells were transfected with pCMV-Cx43 or pGL3-basic in the presence of 1 μM TSA, 1 mM SB or 1 mM 4-PB and incubated for 24 h. The results show caspase-3/7 activity as a percentage of the control (pGL3-basic-transfected cells). Each result represents the mean (n=2).

in GJIC (22.2%) (Fig. 2C), compared with the pGL3-basic-transfected cells. Moreover, in the pCMV-Cx43-transfected cells, TSA, 4-PB and SB did not increase the GJIC (24.2%, 20.0% and 19.4%, respectively) even though they induced the overexpression of Cx43 (Fig. 2D and E). These findings indicated that the transfection of Cx43 with an HDAC inhibitor could not increase the GJIC compared with Cx43 alone.

Next, to examine whether the Cx43 was transported properly to the plasma membrane and formed fluorescent puncta at cell-cell interfaces, we constructed a plasmid encoding a Cx43-EGFP chimera and investigated the localization of Cx43-EGFP protein in the cells. Confocal micrographs revealed that the Cx43-EGFP was localized to the intracellular compartment (Fig. 3A), suggesting that the defect of GJIC in the cells was due to an inability to assemble functional gap junctions. Furthermore, the transport of Cx43-EGFP was not affected by the co-introduction of TSA or 4-PB (Fig. 3B and C). In LNCaP cells, known to form assemblies of functional gap junctions at the membrane on transfection of the Cx43 gene (32). Cx43-EGFP showed the expected localization at sites of contact between the cells (Fig. 3D, arrow), suggesting that the subcellular targeting of Cx43-EGFP was not affected by the tagging with EGFP. From these results, KB cells could not correctly transport Cx43 protein into the membrane, therefore, the GJIC-mediated transfer shown in Fig. 2B might be regulated by another endogenous Cx species. Although functional gap junctions did not form in KB cells transfected with pCMV-Cx43, the expression of Cx43 could induce cell cycle arrest. There is evidence of gap junction-independent roles of Cx in the control of cell growth and the suppression of tumorigenicity (33). This finding suggests that the Cx43 expression in KB cells induced the cell growth inhibition via a GJIC-independent mechanism.

DNA array. To investigate the mechanism of growth inhibition by Cx43, we generated cDNA probes from KB cells transfected with pCMV-Cx43 or pGL3-basic in the presence or absence of TSA or 4-PB for 24 h, and evaluated the effect on the expression of cell cycle-related genes which were among the key genes that affect progression through the cell cycle (Table I). PPIA and GAPDH were used as internal standards. In Cx43-transfected cells, compared with pGL3-basic-transfected cells, the expression of genes involved in the G_1 phase, DNA damage checkpoint, and ATM pathway, was up-regulated. An up-regulated mRNA expression was found in 11 genes in G_1 phase (CDC7, cdk2, p16, Cks1p9, Cullin 2, Cullin 3, Cullin 4B, E2F-4, Nedd8, skp1 and skp2), 2 genes in S phase (CDC6 and CDK7), 2 genes in M phase (MAD2L1 and Rbx-1) and 6 genes involved in the DNA damage checkpoint and ATM pathway (chk1, MRE11A, MRE11B, UBE1, SUMO-1 and E6-AP) (Table I), with a difference of ≥2-fold from pGL3-basic-transfected cells. The introduction of pCMV-

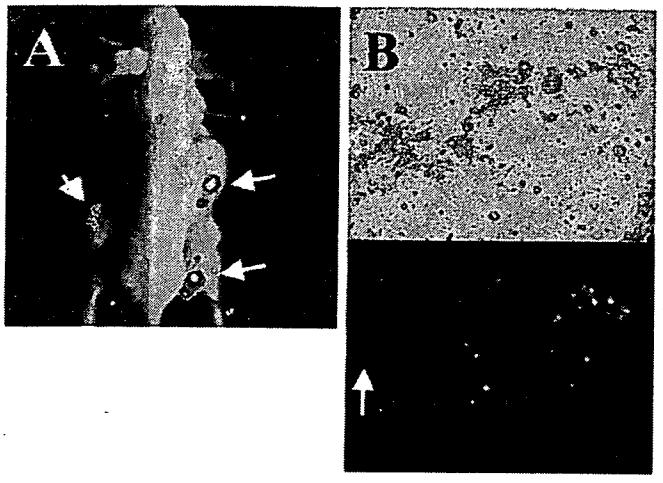

Figure 5. Tumor transfection *in vivo*. Xenografts of KB tumor cells were intratumorally injected with NP-F nanoplex of pCMV-luc (A) or pEGFP-C1 (B). (A) Twenty-four hours after intratumoral injections, mice were imaged and pseudocolor images representing light emitted from tumors superimposed over grayscale reference image of representative mice. (B) Photomicrographs of tumor after cryosection were taken with a x40 objective. Arrow, injection sites.

Cx43 plus 4-PB up-regulated mRNA expression in 2 genes in G_1 phase (CDC7 and skp2), 2 genes in S phase (cyclin G2 and CDK7) and 3 genes involved in the DNA damage checkpoint (MRE11B, nibirin and SUMO-1) compared with that of pCMV-Cx43 alone. The introduction of pCMV-Cx43 plus TSA up-regulated mRNA expression in 1 gene in G_1 phase (CDC7) and 1 gene in S phase (CDK7), compared with that of pCMV-Cx43 alone.

We also assessed the effect of pCMV-Cx43 on the cell cycle 24 h after transfection into KB cells (data not shown). Flow cytometric analysis revealed that transfection of pCMV-Cx43 caused an increase in the percentage of cells in G_1 phase (76%) compared with transfection of pGL3-basic (70%). Co-transfection with 4-PB or SB did not result in a substantial accumulation in G_1 phase induced by Cx43 expression (77%), but that with TSA caused a decrease in the percentage of cells in G_1 phase (58%).

Combined delivery of pCMV-Cx43 with HDAC inhibitors in vitro. HDAC inhibitors including TSA, 4-PB and SB have been used as antineoplastic agents (20). We investigated the cell viability 48 h after treatment with the HDAC inhibitor alone at optimal concentration for increased expression of Cx43 protein. As the result, 1 mM TSA showed high cytotoxicity for the cells (7.3% in cell viability), but 1 mM 4-PB and 1 mM SB did not (71% and 87% in cell viability, respectively) (Fig. 4A). Next, we explored whether the co-introduction of pCMV-Cx43 plus a HDAC inhibitor increased cytotoxicity. The co-introductions of pCMV-Cx43 plus TSA and 4-PB into the cells suppressed significantly tumor growth compared to that of pCMV-Cx43 alone, but pCMV-Cx43 plus SB did not (Fig. 4A). These results suggested that 1 mM 4-PB and 1 μM TSA could induce a high level of Cx43 protein, and could increase suppression of cell growth by the co-introduction of pCMV-Cx43. However, to confirm suppression of tumor growth by overexpressed Cx43, co-introduction of pCMV-Cx43 plus 4-PB was adequate, because 1 μM TSA exhibited strong cytotoxicity without Cx43 expression. Thereafter, we investigated the mechanism of inhibition of cell growth by the co-introduction of pCMV-Cx43 plus 4-PB and applied this combination to xenografts.

Effect of Cx43 with HDAC inhibitors on apoptosis in vitro. Tanaka and Grossman reported that overexpression of Cx26 in human bladder and prostate cancer enhanced the cytotoxicity of chemotherapy by down-regulating the expression of anti-apoptotic bcl-2 (15,16). Therefore, we examined the effect on the expression of bcl-2 mRNA 24 h after the transfection of Cx43 into KB cells by quantitative PCR analysis. pCMV-Cx43 transfection resulted in a down-regulation of bcl-2 mRNA expression compared with pGL3-basic transfection (~64%) (Fig. 4B). Furthermore, the transfection of pCMV-Cx43 plus 4-PB induced a significantly greater down-regulation (~24% of pGL3-basic, respectively) of bcl-2 mRNA expression, whereas 4-PB alone did not.

Next, to examine the effect of Cx43 on the expression of apoptosis-associated enzymes, we measured caspase-3/7 activity 24 h after pCMV-Cx43-transfection with or without HDAC inhibitors (Fig. 4C). Caspase-3/7 activity in pCMV-Cx43-transfected cells was approximately 1.4-fold higher than that in pGL3-basic-transfected cells. The treatments with SB and TSA in pGL3-basic-transfected cells induced a 1.4- and 1.2-fold increase in activity, respectively, compared with pGL3-basic alone, and the co-introduction of pCMV-Cx43 and SB or TSA did not increase the activity (1.4- and 1.3-fold that of levels in pGL3-basic-transfected cells, respectively). In contrast, the treatment with 4-PB in pGL3-basic-transfected cells induced the most potent caspase-3/7 activity (1.7-fold that of activity of pGL3-basic-transfected cells), and the co-introduction of pCMV-Cx43 and 4-PB enhanced the activity (1.9-fold that in pGL3-basic-transfected cells). These findings suggest that combining pCMV-Cx43 with 4-PB might result in an induction of caspase-3/7 activity in the cells.

In vivo transfection. To test the utility of NP-F for gene delivery *in vivo*, we evaluated transfection efficiency by intratumoral injection of NP-F nanoplex of pCMV-luc or pEGFP-C1 into KB tumor xenografts. NP-F induced luciferase expression at a high level around KB tumors (Fig. 5A), however, the distribution of EGFP-expressed cells was restricted to the center of the tumor mass in the vicinity of the injection site (Fig. 5B).

Combination gene therapy in KB tumor xenografts. To evaluate the potential for *in vivo* therapy in KB tumor xenografts, we evaluated the anti-tumor effect by directly injecting the NP-F nanoplex of pCMV-Cx43 or pGL3-basic following a direct injection of 4-PB once a day three times into the xenografts. Yamano *et al* reported that an intratumoral injection of HDAC inhibitor, FR901228, enhanced luciferase expression in solid tumors which were intratumorally injected with luciferase plasmid, whereas the intraperitoneal injection did not (21). Transfection with pCMV-Cx43 alone did not inhibit tumor growth compared with that by pGL3-basic (Fig. 6A). pGL3-basic plus 4-PB treatment moderately suppressed

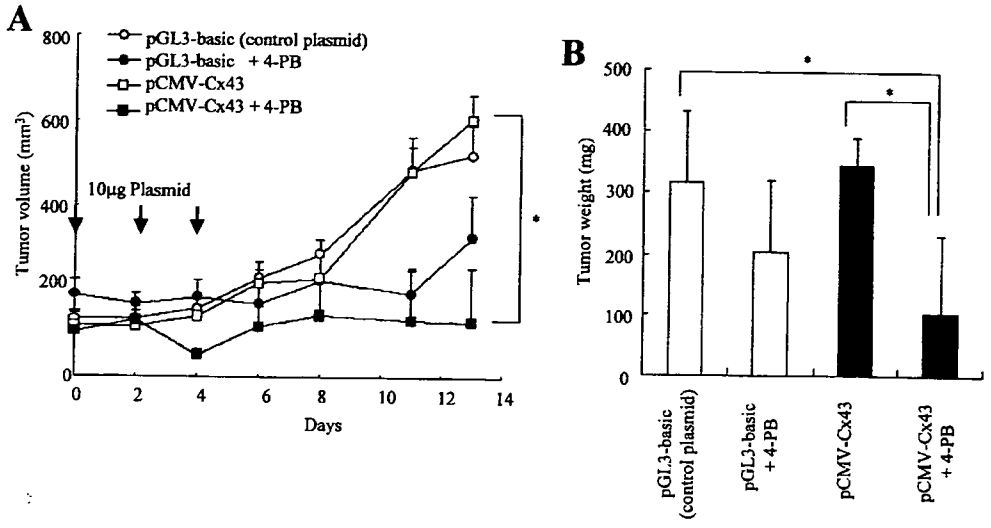

Figure 6. Tumor growth after intratumoral injection of pCMV-Cx43 plus 4-PB. An NP-F nanoplex of 10 μg of pCMV-Cx43 or 10 μg of pGL3-basic was injected on day 0, 2 and 4 with or without 1 mg of 4-PB as described in Materials and methods. Tumor volume was measured and the growth ratio was calculated as an increase in tumor volume (A). Tumor weight when all mice were sacrificed at day 13 (B). The results indicate the mean volume and weight ± SE or SD, respectively (n=4). Statistical significance of the data was evaluated with Fisher's exact test. *P<0.05, compared with the pCMV-Cx43 plus 4-PB.

tumor growth, but the effect was not statistically significant (P>0.05). The introduction of pCMV-Cx43 plus 4-PB significantly suppressed tumor growth, and complete regression was observed in 2 of 4 tumors on day 13 after treatment. A comparison of tumor weight after excision also demonstrated that the tumor growth was significantly attenuated in the mice treated with pCMV-Cx43 plus 4-PB compared with just pGL3-basic (Fig. 6B). Neither the transfection of pCMV-Cx43 alone, the injection of 4-PB alone, nor the introduction of pCMV-Cx43 plus 4-PB altered the change in body weight during 2 weeks of treatment (data not shown).

To determine the fate of tumor cells after gene therapy with pCMV-Cx43, KB tumor xenografts were analyzed by histological examination. The tumors treated with 4-PB showed no evidence of tumor cell death (Fig. 7B) even though the treatment suppressed tumor growth (Fig. 6A and B). Tumors transfected with pCMV-Cx43 exhibited many aggregated cells in the eosinophilic mass although transfection did not suppress tumor growth (Fig. 7C and E). The tumors transfected with pCMV-Cx43 plus 4-PB showed cell death in the eosinophilic mass (Fig. 7D and F). These findings suggested that the introduction of pCMV-Cx43 plus 4-PB had a strong anti-tumor effect on KB tumor xenografts.

Discussion

Restoring Cx expression and/or GJIC in Cx-deficient tumor cells by gene delivery may decrease tumor cell growth (8,11). In the present study, we found that Cx43 expression induced significantly tumor growth inhibition in nasopharyngeal cancer KB cells via a GJIC-independent mechanism. Furthermore, enforced expression of Cx43 by 4-PB enhanced the cell death through activation of the apoptosis pathway, and the combined delivery of Cx43 with 4-PB suppressed the growth of tumor xenografts *in vivo*. This is the first report that enforced expression of Cx43 by 4-PB has potential as a tumor growth inhibitor.

The transfection of pCMV-Cx43 into KB cells inhibited the cell growth (Fig. 1A), but Cx43 was localized to the intracellular compartment (Fig. 3A). Regarding the function of Cx43 in growth inhibition, a truncated Cx43 having the intracellular C-terminal domain of Cx43 could not form gap junctions but inhibited the tumor growth (12), indicating that Cx43 suppresses tumor growth via a GJIC-independent mechanism (33). The mechanistic aspects of the GJIC-independent functions of Cxs remain largely unknown. Several possible mechanisms have been hypothesized (34). In Cx43-transfected cells, we found up-regulated mRNA expression in the G_1 phase and DNA damage checkpoint and ATM pathway genes by cDNA array analysis (Table I). Cx43 transfection induced p16 expression, and the DNA-damage-response by regulating the expression of Mre11A, Mre11B and nibrin, known to be important for mediating ATM-dependent checkpoint pathways (35). p16 is an important regulator of the cell cycle at the G_1 phase (36). The expression of the nibrin and Mre11 genes was induced in an irradiation-evoked DNA damage checkpoint response (37,38), suggesting that the transfection of pCMV-Cx43 had a similar or even identical underlying sensitivity to irradiation, and function in a similar signal pathway, in response to DNA damage. These findings corresponded with the result that Cx43-transfected cells had increased caspase-3/7 activity (Fig. 4C). Seul *et al* reported that the adenoviral delivery of Cx37 induced endothelial cell death through apoptosis (39). Overexpression of Cx43 in KB cells appears to regulate the expression of many genes involved in the G_1 phase of the cell cycle and apoptosis. This is the first report that Cx43 gene delivery induced effective growth inhibition via a GJIC-independent mechanism in KB cells.

Co-introduction of pCMV-Cx43 and TSA, SB or 4-PB into the cells up-regulated the expression of Cx43 protein (Fig. 1B). The amplification of Cx43 expression resulted from an increase in translation from Cx43 mRNA rather than in transcription from pCMV-Cx43. As another possibility,

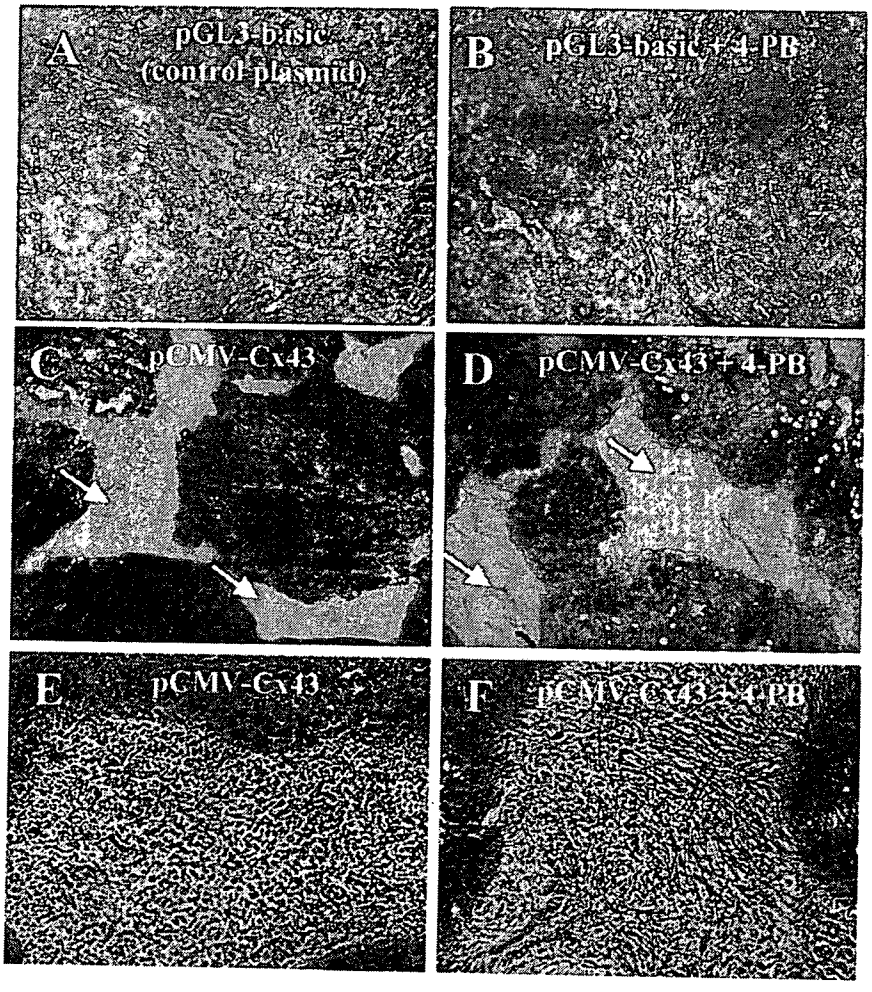

Figure 7. Histological analysis of tumors after Cx43 transfection and/or 4-PB treatment. Tumors were obtained when all mice were sacrificed at day 13. Photomicrographs of hematoxylin and eosin-stained sections of tumors were taken with x40 (A and D) and x100 (E and F) objectives. Tumor injected with 10 μg of pGL3-basic (A), tumor injected with 10 μg of pGL3-basic plus 1 mg 4-PB (B), tumor injected with 10 μg of pCMV-Cx43 (C and E), and tumor injected with 10 μg of pCMV-Cx43 plus 1 mg 4-PB (D and F). Arrowheads: tumor death areas. (E and F) Magnifications of the area of tumor death observed as an eosinophilic mass in C and D, respectively.

the amplified expression might result from an indirect effect on stabilization of Cx43 protein by HDAC inhibitors. Expression of endogenous Cx43 protein in KB cells was also weakly increased when the cells were treated with 4-PB or SB (Fig. 1B). Among the HDAC inhibitors, 4-PB up-regulated the expression of endogenous Cx43 in human gliomas (40,41). Thus, pCMV-Cx43 plus either 4-PB or SB will be greater inducers for endogenous and exogenous Cx43 expression in nasopharyngeal tumors.

Combining pCMV-Cx43 with 4-PB or TSA in the cells enhanced the cytotoxicity, but that with SB did not (Fig. 4A). Several groups have reported that combining Cx gene therapy with a chemotherapeutic agent resulted in greater suppression of tumor growth (14,15). Cx43 expression could enhance the sensitivity of human glioblastoma cells to doxorubicin, paclitaxel and etoposide (14). Transfection with the Cx26 gene induced down-regulation of bcl-2 expression in prostate cancer cells (15). Transfection of pCMV-Cx43 induced down-regulation of bcl-2 expression in prostate cancer PC-3 cells, and increased sensitivity to docetaxel (42). In this study, the introduction of pCMV-Cx43 plus 4-PB in KB cells resulted in greater reduction of bcl-2 mRNA expression and induced caspase-3/7 activity (Fig. 4B and C). From the result obtained with the cDNA array, the co-introduction of 4-PB up-regulated mRNA expression in DNA damage checkpoint-related genes such as MRE11B, nibirin and SUMO-1 (Table I), suggesting an enhancement of the signal pathway in response to DNA damage. Furthermore, on the overexpression of Cx43 by 4-PB, strong expression of p16 protein was observed (Table I). Transfection of the p16 gene into nasopharyngeal carcinoma increased sensitivity to chemotherapeutic drugs such as 5FU and cisplatin (43). Therefore, the possible mechanism of enhanced efficacy with pCMV-Cx43 plus 4-PB might result from the effect of Cx43 overexpressed by 4-PB to induce growth inhibition and the effect on increased cytotoxicity of 4-PB by down-regulating bcl-2 expression. This may provide valuable molecular therapeutic information to improve the clinical applications of both HDAC inhibitors and Cx43 gene therapy.

The introduction of pCMV-Cx43 plus TSA also resulted in significant reduction of tumor growth (Fig. 4A). However, from DNA array analysis, the introduction of pCMV-Cx43 plus

TSA slightly affected mRNA expression of genes involved in DNA damage checkpoint and ATM pathway, compared with that of pCMV-Cx43 alone (Table I). These findings suggested that the mechanism of induction of apoptosis might be different between TSA and 4-PB. However, it was not clear why different responses to 4-PB and TSA in the induction of genes involved in the cell cycle, DNA damage checkpoint, and ATM pathway were observed.

In *in vivo* Cx43 gene therapy, pCMV-Cx43 could not suppress the growth of KB tumor xenografts (Fig. 6A), but the tumors exhibited cell death (Fig. 7C and E). The observed restricted cell death in tumors may be due to the effect of Cx43 since the distribution of Cx expression by NP-F transfection into tumors was restricted to the center of the tumor mass in the vicinity of the injection site (Fig. 5B). Therefore, to induce inhibition of tumor growth by Cx43 expression alone, it is necessary to develop a gene carrier with the ability to introduce DNA widely into the tumor. 4-PB with pGL3-basic suppressed tumor growth, but the tumors exhibited no evidence of cell death (Fig. 7B). HDAC inhibitors including 4-PB have been reported to inhibit the process of new capillary blood vessel formation or tumor angiogenesis, in addition to the inhibitory effect on cancer cell proliferation (44-46). The reduction in tumor size may be due to the antitumor effects of 4-PB. The combination of pCMV-Cx43 and 4-PB suppressed significantly tumor growth and weight *in vivo* compared with the control (Fig. 6), and resulted in massive tumor cell death (Fig. 7D and F), suggesting that the combined delivery showed a synergistic or additive effect in terms of growth inhibition and tumor toxicity. One explanation for enhanced growth inhibition by combination therapy might be that Cx43 increased sensitivity for 4-PB via the down-regulation of bcl-2. As another possibility, the reduction in tumor size by 4-PB may increase the transfection efficiency of pCMV-Cx43, because significant tumor growth inhibition by intratumoral injection was obtained in tumor gene therapy when the tumor volume was <50 mm^3 (47). The combination of pCMV-Cx43 and an HDAC inhibitor transfected with NP-F has great potential as a tumor-targeted carrier for *in vivo* cancer gene therapy.

In conclusion, we demonstrated that Cx43 transfected by nanoparticle had a tumor suppressive effect via a mechanism that was independent of GJIC in KB cells, and combining pCMV-Cx43 with 4-PB resulted in significantly greater growth suppression of the cells and xenografts. Thus, the combination of Cx43 expression and an HDAC inhibitor may serve as a novel tool for gene therapy.

Acknowledgements

This project was supported in part by a grant from the Promotion and Mutual Aid Corporation for Private Schools of Japan, and by a Grant-in-Aid for Scientific Research from the Ministry of Education, Culture, Sports, Science, and Technology of Japan.

References

1. Vine AL and Bertram JS: Cancer chemoprevention by connexins. Cancer Metastasis Rev 21: 199-216, 2002.
2. Yamasaki H and Naus CC: Role of connexin genes in growth control. Carcinogenesis 17: 1199-1213, 1996.
3. Lee SW, Tomasetto C, Paul D, Keyomarsi K and Sager R: Transcriptional downregulation of gap-junction proteins blocks junctional communication in human mammary tumor cell lines. J Cell Biol 118: 1213-1221, 1992.
4. Tomasetto C, Neveu MJ, Daley J, Horan PK and Sager R: Specificity of gap junction communication among human mammary cells and connexin transfectants in culture. J Cell Biol 122: 157-167, 1993.
5. Habermann H, Ray V, Habermann W and Prins GS: Alterations in gap junction protein expression in human benign prostatic hyperplasia and prostate cancer. J Urol 167: 655-660, 2002.
6. Huang RP, Hossain MZ, Sehgal A and Boynton AL: Reduced connexin43 expression in high-grade human brain glioma cells. J Surg Oncol 70: 21-24, 1999.
7. Sawey MJ, Goldschmidt MH, Risek B, Gilula NB and Lo CW: Perturbation in connexin 43 and connexin 26 gap-junction expression in mouse skin hyperplasia and neoplasia. Mol Carcinog 17: 49-61, 1996.
8. Zhang ZQ, Zhang W, Wang NQ, Bani-Yaghoub M, Lin ZX and Naus CC: Suppression of tumorigenicity of human lung carcinoma cells after transfection with connexin43. Carcinogenesis 19: 1889-1894, 1998.
9. Oyamada Y, Oyamada M, Fusco A and Yamasaki H: Aberrant expression, function and localization of connexins in human esophageal carcinoma cell lines with different degrees of tumorigenicity. J Cancer Res Clin Oncol 120: 445-453, 1994.
10. Pelin K, Hirvonen A and Linnainmaa K: Expression of cell adhesion molecules and connexins in gap junctional intercellular communication deficient human mesothelioma tumour cell lines and communication competent primary mesothelial cells. Carcinogenesis 15: 2673-2675, 1994.
11. Mehta PP, Perez-Stable C, Nadji M, Mian M, Asotra K and Roos BA: Suppression of human prostate cancer cell growth by forced expression of connexin genes. Dev Genet 24: 91-110, 1999.
12. Zhang YW, Kaneda M and Morita I: The gap junction-independent tumor-suppressing effect of connexin 43. J Biol Chem 278: 44852-44856, 2003.
13. Nicholas TW, Read SB, Burrows FJ and Kruse CA: Suicide gene therapy with Herpes simplex virus thymidine kinase and ganciclovir is enhanced with connexins to improve gap junctions and bystander effects. Histol Histopathol 18: 495-507, 2003.
14. Huang RP, Hossain MZ, Huang R, Gano J, Fan Y and Boynton AL: Connexin 43 (cx43) enhances chemotherapy-induced apoptosis in human glioblastoma cells. Int J Cancer 92: 130-138, 2001.
15. Tanaka M and Grossman HB: Connexin 26 induces growth suppression, apoptosis and increased efficacy of doxorubicin in prostate cancer cells. Oncol Rep 11: 537-541, 2004.
16. Tanaka M and Grossman HB: Connexin 26 gene therapy of human bladder cancer: induction of growth suppression, apoptosis, and synergy with Cisplatin. Hum Gene Ther 12: 2225-2236, 2001.
17. Peart MJ, Tainton KM, Ruefli AA, *et al*: Novel mechanisms of apoptosis induced by histone deacetylase inhibitors. Cancer Res 63: 4460-4471, 2003.
18. Blagosklonny MV, Robey R, Sackett DL, *et al*: Histone deacetylase inhibitors all induce p21 but differentially cause tubulin acetylation, mitotic arrest, and cytotoxicity. Mol Cancer Ther 1: 937-941, 2002.
19. Ishiguro K and Sartorelli AC: Activation of transiently transfected reporter genes in 3T3 Swiss cells by the inducers of differentiation/apoptosis-dimethylsulfoxide, hexamethylene bisacetamide and trichostatin A. Eur J Biochem 271: 2379-2390, 2004.
20. Piekarz R and Bates S: A review of depsipeptide and other histone deacetylase inhibitors in clinical trials. Curr Pharm Des 10: 2289-2298, 2004.
21. Yamano T, Ura K, Morishita R, Nakajima H, Monden M and Kaneda Y: Amplification of transgene expression *in vitro* and *in vivo* using a novel inhibitor of histone deacetylase. Mol Ther 1: 574-580, 2000.
22. Imanishi R, Ohtsuru A, Iwamatsu M, *et al*: A histone deacetylase inhibitor enhances killing of undifferentiated thyroid carcinoma cells by p53 gene therapy. J Clin Endocrinol Metab 87: 4821-4824, 2002.
23. Takimoto R, Kato J, Terui T, *et al*: Augmentation of antitumor effects of p53 gene therapy by combination with HDAC inhibitor. Cancer Biol Ther 4: 421-428, 2005.
24. Yamamoto S, Yamano T, Tanaka M, *et al*: A novel combination of suicide gene therapy and histone deacetylase inhibitor for treatment of malignant melanoma. Cancer Gene Ther 10: 179-186, 2003.

25. Parker N, Turk MJ, Westrick E, Lewis JD, Low PS and Leamon CP: Folate receptor expression in carcinomas and normal tissues determined by a quantitative radioligand binding assay. Anal Biochem 338: 284-293, 2005.
26. Hattori Y and Maitani Y: Folate-linked lipid-based nanoparticle for targeted gene delivery. Curr Drug Delivery 2: 243-252, 2005.
27. Hattori Y, Kubo H, Higashiyama K and Maitani Y: Folate-linked nanoparticles formed with DNA complexes in sodium chloride solution enhance transfection efficiency. J Biomed Nanotech 1: 176-184, 2005.
28. Hattori Y and Maitani Y: Folate-linked nanoparticle-mediated suicide gene therapy in human prostate cancer and nasopharyngeal cancer with herpes simplex virus thymidine kinase. Cancer Gene Ther 12: 796-809, 2005.
29. Robe PA, Jolois O, N'Guyen M, *et al*: Modulation of the HSV-TK/ganciclovir bystander effect by n-butyrate in glioblastoma: correlation with gap-junction intercellular communication. Int J Oncol 25: 187-192, 2004.
30. Hattori Y and Maitani Y: Enhanced *in vitro* DNA transfection efficiency by novel folate-linked nanoparticles in human prostate cancer and oral cancer. J Control Release 97: 173-183, 2004.
31. Bartova E, Pachernik J, Harnicarova A, *et al*: Nuclear levels and patterns of histone H3 modification and HP1 proteins after inhibition of histone deacetylases. J Cell Sci 118: 5035-5046, 2005.
32. Govindarajan R, Zhao S, Song XH, *et al*: Impaired trafficking of connexins in androgen-independent human prostate cancer cell lines and its mitigation by alpha-catenin. J Biol Chem 277: 50087-50097, 2002.
33. Jiang JX and Gu S: Gap junction- and hemichannel-independent actions of connexins. Biochim Biophys Acta 1711: 208-214, 2005.
34. Zhang YW, Nakayama K, Nakayama K and Morita I: A novel route for connexin 43 to inhibit cell proliferation: negative regulation of S-phase kinase-associated protein (Skp 2). Cancer Res 63: 1623-1630, 2003.
35. Lee JH and Paull TT: ATM activation by DNA double-strand breaks through the Mre11-Rad50-Nbs1 complex. Science 308: 551-554, 2005.
36. Shapiro GI, Edwards CD and Rollins BJ: The physiology of p16(INK4A)-mediated G1 proliferative arrest. Cell Biochem Biophys 33: 189-197, 2000.
37. Desai-Mehta A, Cerosaletti KM and Concannon P: Distinct functional domains of nibrin mediate Mre11 binding, focus formation, and nuclear localization. Mol Cell Biol 21: 2184-2191, 2001.
38. Gatei M, Young D, Cerosaletti KM, *et al*: ATM-dependent phosphorylation of nibrin in response to radiation exposure. Nat Genet 25: 115-119, 2000.
39. Seul KH, Kang KY, Lee KS, Kim SH and Beyer EC: Adeno-viral delivery of human connexin37 induces endothelial cell death through apoptosis. Biochem Biophys Res Commun 319: 1144-1151, 2004.
40. Asklund T, Appelskog IB, Ammerpohl O, Ekstrom TJ and Almqvist PM: Histone deacetylase inhibitor 4-phenylbutyrate modulates glial fibrillary acidic protein and connexin 43 expression, and enhances gap-junction communication, in human glioblastoma cells. Eur J Cancer 40: 1073-1081, 2004.
41. Ammerpohl O, Thormeyer D, Khan Z, *et al*: HDACi phenylbutyrate increases bystander killing of HSV-tk transfected glioma cells. Biochem Biophys Res Commun 324: 8-14, 2004.
42. Fukushima M, Hattori Y, Yoshizawa T and Maitani Y: Combination of non-viral connexin 43 gene therapy and docetaxel inhibits the growth of human prostate cancer in mice. Int J Oncol 30: 225-231, 2007.
43. Chow LS, Wang X, Kwong DL, Sham JS, Tsao SW and Nicholls JM: Effect of p16INK4a on chemosensitivity in nasopharyngeal carcinoma cells. Int J Oncol 17: 135-140, 2000.
44. Pili R, Kruszewski MP, Hager BW, Lantz J and Carducci MA: Combination of phenylbutyrate and 13-cis retinoic acid inhibits prostate tumor growth and angiogenesis. Cancer Res 61: 1477-1485, 2001.
45. Williams RJ: Trichostatin A, an inhibitor of histone deacetylase, inhibits hypoxia-induced angiogenesis. Expert Opin Investig Drugs 10: 1571-1573, 2001.
46. Kim MS, Kwon HJ, Lee YM, *et al*: Histone deacetylases induce angiogenesis by negative regulation of tumor suppressor genes. Nat Med 7: 437-443, 2001.
47. Galaup A, Opolon P, Bouquet C, *et al*: Combined effects of docetaxel and angiostatin gene therapy in prostate tumor model. Mol Ther 7: 731-740, 2003.

Available online at www.sciencedirect.com
ScienceDirect
Journal of Controlled Release 117 (2007) 281–290
journal of controlled release
www.elsevier.com/locate/jconrel
GENE DELIVERY

Mechanisms of co-modified liver-targeting liposomes as gene delivery carriers based on cellular uptake and antigens inhibition effect

Yuan Zhang [a], Xian Rong Qi [a,*], Yan Gao [b], Lai Wei [b], Yoshie Maitani [c], Tsuneji Nagai [c]

[a] *School of Pharmaceutical Sciences, Peking University, Beijing 100083, China*
[b] *Institute of Hepatology, Peking University People's Hospital, Beijing 100044, China*
[c] *Institute of Medicinal Chemistry, Hoshi University, Ebara 2-4-41, Shinagawa-Ku, Tokyo 142-8501, Japan*

Received 26 March 2006; accepted 9 November 2006
Available online 16 November 2006

Abstract

In order to deliver antisense oligonucleotides (asODN) into hepatocytes orientedly in the treatment of hepatitis B virus (HBV) infection, the liver-targeting cationic liposomes was developed as a gene carrier, which was co-modified with the ligand of the asialoglycoprotein receptor (ASGPR), β-sitosterol-β-D-glucoside (sito-G) and the nonionic surfactant, Brij 35. Flow cytometry (FCM) analysis and enzyme-linked immunosorbent assay (ELISA) showed that the asODN-encapsulating cationic liposomes exhibited high transfection efficiency and strong antigens inhibition effect in primary rat hepatocytes and HepG2.2.15 cells, respectively. With the help of several inhibitors acting on different steps during the targeting lipofection, the cellular uptake mechanisms of the co-modified liver-targeting cationic liposomes were investigated through antigens inhibition effect assay and confocal laser scanning microscopy (CLSM) analysis. The cellular uptake with high transfection efficiency seemed to involve both endocytosis and membrane fusion. The ligand sito-G was confirmed to be able to enhance ASGPR-mediated endocytosis, the nonionic surfactant Brij 35 seemed to be able to facilitate membrane fusion, and the co-modification resulted in the most efficient transfection but no enhanced cytotoxicity. These results suggested that the co-modified liver-targeting cationic liposomes would be a specific and effective carrier to transfer asODN into hepatocytes infected with HBV orientedly.

Keywords: β-sitosterol-β-D-glucoside; Liver-targeting; Co-modified cationic liposomes; Membrane fusion; Endocytosis

1. Introduction

In order to transfer the therapeutic asODN effectively into the cells both in vitro and in vivo, various gene carriers have been developed by many groups [1,2]. Among those, the cationic liposomes is one kind of widely used non-viral carriers with high transfection efficiency in vitro, convenient availability, and good flexibility which allows modifications to meet different requirements. However, for successful in vivo applications, it still needs to be improved in the aspects of transfection efficiency, cytotoxicity, targeting delivery, half-life time, etc. [3,4].

Many studies have confirmed the anti-HBV effects of different asODN, and as a new prospective method, anti-HBV gene therapy has attracted much attention [5–7]. Since HBV only infects the hepatocytes rather than nonparenchymal cells in the liver [8], the oriented delivery to hepatocytes would increase the transfection efficiency and decrease the cytotoxicity of the asODN and the cationic liposomes theoretically. ASGPR-mediated endocytosis was known to be an efficient liver-targeting pathway. There are several galactose- or lactose-terminated compounds such as asialoorosomucoid [9], galactosylated poly-L-glutamic acid [10], asialofetuin glycopeptide [11], lactosylceramide [12] etc., to be used as the target ligands in the liver-targeting liposomes, polymers or nanoparticles [13]. Sito-G is the major component of soybean sterylglucoside (SG), a kind of plant extract mixture with all the components containing one glucose residue [14]. Both SG and sito-G could be recognized specifically by ASGPR and the neutral liposomes containing SG or sito-G could target the liver [14,15]. Meanwhile, SG and sito-G are abundant and inexpensive, which was advantageous for them to be developed as a liver-

* Corresponding author. Tel.: +86 10 82801584; fax: +86 10 82802791.
E-mail address: qixr2001@yahoo.com.cn (X. Rong Qi).

0168-3659/$ - see front matter © 2006 Elsevier B.V. All rights reserved.
doi:10.1016/j.jconrel.2006.11.006

targeting ligand, because most of the other ligands mentioned above were expensive to synthesize and purify. Hwang et al. reported the cationic liposomes containing sito-G as the liver-targeting gene delivery carrier and enhanced transfection efficiency by sito-G [16]. We also reported that the cationic liposomes containing SG showed liver-targeting effect [17]. Nonionic surfactants, for example, Tween 80, had improved the transfection efficiency of cationic emulsions although the mechanisms were unclear [18]. In the preliminary study, we compared the transfection enhancement towards the cationic liposomes by the different modifications with several nonionic surfactants such as Tween 80, Span 80, Brij 35 etc., and Brij 35 showed to be the most efficient one.

In this study, we designed the novel cationic liposomes co-modified with sito-G and Brij 35, to enhance the delivery of a 15-mer anti-HBV asODN orientedly to the hepatocytes, and evaluated the transfection efficiency and the antigen inhibition effect (i.e. inhibitory effect of asODN to virus antigens production) of the encapsulated asODN in vitro. For the successful design and optimization of cationic liposomes, there are many intricate steps to be considered for the cellular uptake of asODN mediated by the cationic liposomes [4,19]. In this study, with the help of some inhibitors that could act on different steps of the cellular uptake, such as asialofetuin, wortmannin and nigericin, the cellular uptake mechanisms and intracellular distributions of both cationic liposomes and encapsulated asODN were analyzed based on the antigens inhibition effect, FCM and CLSM.

2. Materials and methods

2.1. Materials

Dipalmitoyl-phosphatidylcholine (DPPC) was supplied by NOF Corporation (Tokyo, Japan). Dioleoyl-phosphatidylethanolamine (DOPE) was purchased from Northern Lipids (Vancouver, Canada) and rhodamine-DOPE was synthesized by our laboratory. 3β[*N*-(*N*′,*N*′-dimethylaminoethane)-carbamoyl] cholesterol (DC-Chol) was synthesized by our laboratory [20]. Sito-G was isolated and purified from the SG mixture by HPLC in our laboratory. Brij 35 was purchased from Serva (Heidelberg, Germany). Asialofetuin (type I from fetal calf serum), wortmannin and nigericin were purchased from Sigma-Aldrich (St. Louis, USA). Dulbecco's modified Eggle's medium (DMEM) and William's E medium were purchased from Gibco BRL/Life Technologies (New York, NY, USA). Fetal bovine serum (FBS) was purchased from Tianjin Caihui Technologies (Tianjin, China). HepG2.2.15 cells were provided by Hepatology Institute, Peking University People's Hospital (Beijing, China). Male Wistar rats with the body weight 150 g–200 g were purchased from Laboratory Animal Center, Peking University Health Science Center.

2.2. Cells culture

The HepG2.2.15 cells, a human hepatoblastoma cell line which was integrated with the HBV DNA into the chromosome and could stably produce HBV in the culture system, were cultured in WPS-DMEM (DMEM containing 10% (v/v) heat-inactivated FBS, 1% (w/v) penicillin and streptomycin) in the humidified atmosphere with 5% CO_2 at 37 °C. For the treatment with cationic liposomes, the cells at not more than passage 20 were plated with the density of about $4\times10^4/cm^2$ and then incubated for 1 or 2 days till the cell confluence reached at least 70%.

Primary rat hepatocytes were isolated and cultured based on the Seglen two-steps method with some modifications [21]. The prepared hepatocytes were cultured in the MWEM (the modified William's E medium).

2.3. Oligonucleotides

The 15-mer phosphorothioate oligonucleotides (asODN) which had the anti-HBV sequence 5′>GAT GAC TGT CTC TTA<3′, aimed at cap site/SP II of the HBV mRNA, was synthesized on a solid phase DNA synthesizer (PE-ABI 391EP, USA) by phosphite-triester method and was purified by SDS-PAGE. For the FCM and CLSM analysis, the asODN was still labelled on the 5′ end with fluorescin isothiocyanate (FITC).

2.4. Preparation of cationic liposomes

Cationic liposomes encapsulating asODN or FITC-asODN were prepared by film dispersion method as described in the previous study [17]. The liposomes, CL (DPPC:DC-Chol= 20:10), CL/sito-G (DPPC:DC-Chol:sito-G=20:10:1.34), CL/Brij 35 (DPPC:DC-Chol:Brij 35=20:10:1.34), and CL/Brij 35/sito-G (DPPC:DC-Chol:Brij 35:sito-G=20:10:1.34:1.34) were prepared respectively (all the ratios in the formulations above were molar ratios). The stock concentration of asODN or FITC-asODN and the total lipids in the cationic liposome suspension were 28.8 μM and 0.9 mg/mL respectively. Before administrated to the cells, the liposomes were diluted by NPS-DMEM (DMEM containing 10% serum and no penicillin–streptomycin) to the final concentration, expressed as the concentration of the encapsulated asODN. The particle size, zeta potential, and polydispersion index of CL/Brij 35/sito-G were about 155 nm, 30.0 mV and 0.191, respectively, determined by Zeta-Sizer (Malvern, UK).

2.5. Flow cytometry analysis

Primary rat hepatocytes were prepared and plated onto the 24-well plate with the density of 2×10^5 cell/well. After incubation for 2 or 3 days when the cells were growing well, the cells were washed once with MWEM, followed by the addition of the cationic liposomes encapsulating FITC-asODN or free FITC-asODN solution at each given concentration. After incubation for the scheduled time, the cells were detached from the culture plate with 4% (w/v) trypsinase solution and washed three times with PBS by centrifuging at 1000 r/min for 5 min. Finally the cells were suspended in PBS and fixed with the FCM fix solution (containing formalin 1 mL, glucose 2 g, sodium azide 0.2 g, PBS to 100 mL). Then the cell suspension

(more than 10000 cells) was stored at 4 °C for FCM analysis (Beckton Dickinson, Belgium).

2.6. Determination of HBsAg and HBeAg production

HepG2.2.15 cells were plated. The asODN-encapsulating cationic liposomes or the free asODN solution was added with the given concentrations. The treatment agents were refreshed every 24 h for 3 days with the unchanged concentration. The solutions dropped out from the culture wells were collected for the HBsAg (hepatitis B surface antigen) and HBeAg (hepatitis B e antigen) determination. HBsAg and HBeAg productions were determined by ELISA using Akzo Nobel HBsAg ELISA kit (Biomerius, France) and Radim HBeAg ELISA Test System (Radim, Italy), respectively. All the results were expressed as the optical density at 450 nm [OD (450 nm)].

In order to investigate the cellular uptake mechanisms of the encapsulated asODN in CL/Brij 35/sito-G, the inhibitors like asialofetuin, wortmannin and nigericin were added into the medium with the final concentrations 1.0 mg/mL, 0.1 μM and 1.0 μM, respectively, 10 min before the treatment with the asODN-encapsulating cationic liposomes. Then the HBsAg and HBeAg productions were determined as described above.

2.7. Cytotoxicity assay

The cytotoxicity of the modified cationic liposomes encapsulating asODN was determined by MTT assay. The cationic liposomes encapsulating asODN were added at the given concentrations. After incubation for 72 h without refreshing the medium, 20 μL MTT solution (5 g/L) dissolved with PBS buffer (pH 7.2) was added in and then the cells were incubated for 4 h to allow the production of the dark-blue formazan crystal. Then 200 μL of dimethylsulfoxide was added into each well. When the formazan crystal was dissolved completely, the optical density at 490 nm [OD (490 nm)] was determined by a microplate reader. The viability of the treated cells was defined as follow:

The cell viability=OD (490 nm) of the treated cells/OD (490 nm) of the non-treated cells.

2.8. Fluorescent microscopy and confocal laser scanning microscopy analysis

Primary rat hepatocytes were prepared and plated with the density of 4×10^5 cell/well onto the 6-well plate with a cover glass (22 mm×26 mm) in each well. After incubation for 2 or 3 days, the cells were washed once with MWEM, followed by the addition of the cationic liposomes containing rhodamine-DOPE (1%, molar ratio in liposome formulation) and encapsulating FITC-asODN at the given concentrations. After incubation for the scheduled time, 5 μL Hoechst 33258 (1 mg/mL) was added into the medium to stain the nuclear for 30 min. Then the cells on the cover glass were washed for 3 times with PBS, fixed with 4% paraformaldehyde (dissolved with PBS) for 15 min, and then stored at −20 °C for fluorescence microscopy (Olympus, Japan) or confocal laser scanning microscopy (Leica, Germany) analysis.

3. Results

3.1. Transfection efficiency of asODN

To investigate the transfection efficiency of cationic liposomes in primary rat hepatocytes, the cellular uptake of the FITC-asODN was evaluated by FCM. When treated for 6 h with free FITC-asODN solution at 0.36 μM, the primary rat hepatocytes exhibited 10.9% transfection efficiency. Compared to free FITC-asODN solution, the modified cationic liposomes encapsulating FITC-asODN (CL/sito-G, CL/Brij 35 and CL/Brij 35/sito-G) increased transfection efficiency by 4.4- 7.1 folds, but the unmodified cationic liposomes (CL) increased only 1.0 fold (transfection efficiency of 21.9%). In the case of CL/Brij 35 and CL/sito-G, the transfection efficiency values (60.0% and 59.0%) were similar to each other. CL/Brij 35/sito-G, the liver-targeting cationic liposomes co-modified with sito-G and Brij 35, exhibited the strongest transfection efficiency (88.7%). The mean fluorescence intensity (MFI) of CL/Brij 35/sito-G reached the maximum at 6 h and the MFI value at 6 h was almost as much as that at 24 h (Fig. 1a), indicating that the cellular uptake of asODN was time-dependent at the initial period of 6 h and then maintained nearly a constant. Furthermore, from the data with 6 h treatment at various FITC-asODN concentrations, the cellular uptake of asODN was concentration-dependant, and when the FITC-asODN concentration increased to 1.80 μM, the transfection efficiency reached almost 100% (Fig. 1b).

3.2. Biological effect on HBV antigens production

HBsAg and HBeAg, two antigens produced with the progress of HBV infection, are diagnosis indicators of chronic hepatitis B. When the HBsAg or HBeAg level is up or down, the corresponding optical density [OD (450 nm)] will increase or decrease in the antigen production determination, so the antigen level (HBsAg or HBeAg production) can be expressed as OD (450 nm). Here we defined the term "antigen inhibition effect" to describe the inhibitory effect of asODN to HBV antigen production level, which represented the biological effect on HBV antigens production. As shown in Fig. 2, after 3 days treatment with 3.6 μM asODN, CL/Brij 35/sito-G brought the most reduction of antigens production (both HBsAg and HBeAg) of HepG2.2.15 cells and therefore showed the strongest antigen inhibition effects. CL/Brij 35 and CL/sito-G brought more reduction in HBsAg production than CL (Fig. 2a). As for the HBeAg production (Fig. 2b), compared with no treatment group and free asODN solution, both CL/Brij 35 and CL/Brij 35/sito-G showed significant inhibition on HBeAg production, while neither CL nor CL/sito-G did. Although the transfection efficiencies of CL/Brij 35 and CL/sito-G were similar to each other, the antigens inhibition effect of the former was stronger than that of the latter. The difference in the HBsAg and HBeAg production might respect to the complementary

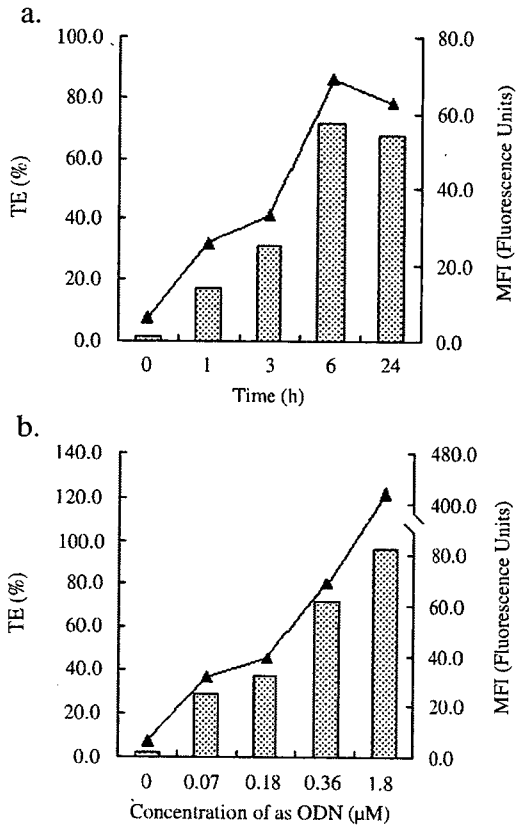

Fig. 1. Transfection activity at (a) different treatment time with 0.36 μM FITC-asODN and (b) different FITC-asODN concentrations with 6 h treatment when treated with FITC-asODN-encapsulating CL/Brij 35/sito-G by flow cytometry. Here TE (bar) referred to transfection efficiency (%), defined as the percentage of the positive cells whose fluorescence intensity was more than 10 intensity units; MFI (line) referred to mean fluorescence intensity (fluorescence units), defined as the arithmetical mean of the fluorescence intensity of all the counted cells. Values represented as mean of two independent experiments.

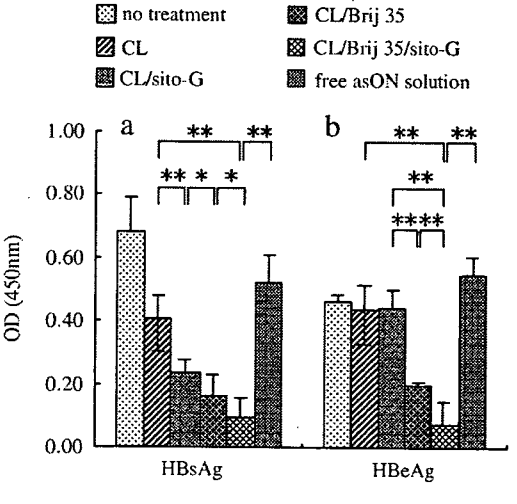

Fig. 2. HBsAg (a) and HBeAg (b) production of HepG2.2.15 cells treated with differently modified cationic liposomes encapsulating asODN and free asODN solution respectively for 3 days. The concentration of asODN was 3.6 μM. OD (450 nm) indicated HBsAg and HBeAg levels. Each value represented the mean± S.D. (n=3). *P<0.05, **P<0.01, significantly different.

sequence of the used asODN. The complementary sequence of this asODN was located in the cap site of 3.5 kb mRNA (involved in the transcription of HBsAg) and the middle site of 2.4 kb mRNA (involved in the transcription of HBeAg) at the same time [8]. It was easier for the cap site to be bound by asODN than the middle site, so HBsAg level was inhibited more than HBeAg level, i.e., the HBsAg inhibition would be more significant.

The relationship between the antigens production inhibition to HepG2.2.15 cells and the concentration of the asODN encapsulated in CL/Brij 35 /sito-G was determined. In the range of 0.18–7.2 μM, the HBsAg production [OD (450 nm)]-concentration curve was an exponential one: (OD (450 nm)= $-0.187 \cdot \mathrm{Ln}C_{\mathrm{asODN}}+0.445$, $r^2=0.987$) (Fig. 3a), and the HBeAg production [OD (450 nm)]-concentration curve was in shape of counter-S (Fig. 3b): OD (450 nm)=$(146.3+0.44 \cdot C_{\mathrm{asODN}}^{6.7})/(146.3+C_{\mathrm{asODN}}^{6.7})$ ($r^2=0.955$). These findings suggested that the HBsAg and HBeAg inhibition effects were concentration-dependant, but after the asODN concentration increased to a certain level, the inhibition effects were strengthened little with the increase of the asODN concentration.

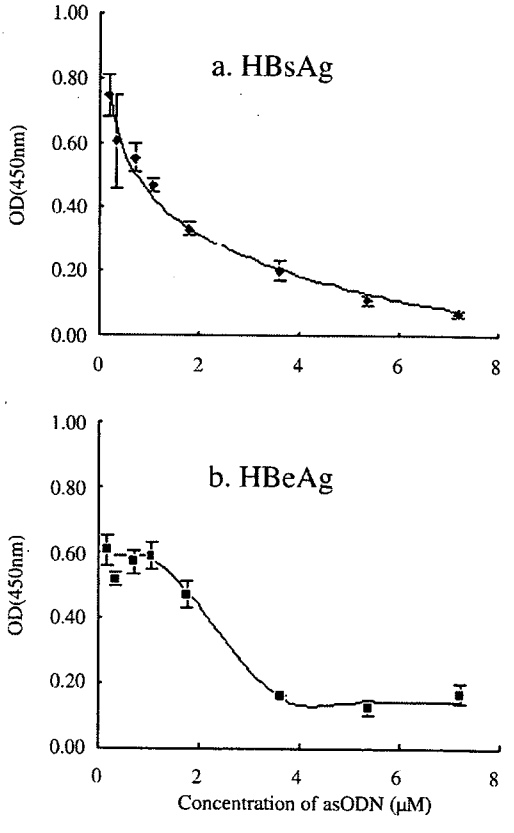

Fig. 3. Relationship between HBsAg (a) and HBeAg (b) production and concentration of asODN encapsulated in CL/Brij 35/sito-G. HepG2.2.15 cells were treated with the cationic liposomes at the asODN concentration from 0 to 7.2 μM for 3 days. In both figures, OD (450 nm) indicated HBsAg and HBeAg level. The line meant the estimation curve: a. HBsAg, OD(450 nm)= $-0.187 \cdot \mathrm{Ln}C_{\mathrm{asODN}}+0.445$, $r^2=0.987$); b. HBeAg, OD(450 nm)=$(146.3+0.44 \cdot C_{\mathrm{asODN}}^{6.7})/(146.3+C_{\mathrm{asODN}}^{6.7})$ ($r^2=0.955$). Each value represented the mean± S.D. (n=3).